

# Particle alignments and shape coexistence in $^{66}\text{Ge}$ and $^{68}\text{Ge}$

M. Hasegawa<sup>1</sup>, K. Kaneko<sup>2</sup> and T. Mizusaki<sup>3</sup>

<sup>1</sup>*Laboratory of Physics, Fukuoka Dental College, Fukuoka 814-0193, Japan*

<sup>2</sup>*Department of Physics, Kyushu Sangyo University, Fukuoka 813-8503, Japan*

<sup>3</sup>*Institute of Natural Sciences, Senshu University, Kawasaki, Kanagawa, 214-8580, Japan*

(Dated: January 27, 2020)

The structure of the  $N \approx Z$  nuclei  $^{66}\text{Ge}$  and  $^{68}\text{Ge}$  is studied by the shell model on a spherical basis. The calculations with an extended  $P + QQ$  Hamiltonian in the configuration space ( $2p_{3/2}$ ,  $1f_{5/2}$ ,  $2p_{1/2}$ ,  $1g_{9/2}$ ) succeed in reproducing experimental energy levels, moments of inertia and  $Q$  moments in Ge isotopes. Using the reliable wave-functions, this paper investigates particle alignments and nuclear shapes in  $^{66}\text{Ge}$  and  $^{68}\text{Ge}$ . It is shown that structural changes in the four sequences of the positive- and negative-parity yrast states with even  $J$  and odd  $J$  are caused by various types of particle alignments in the  $g_{9/2}$  orbit. The coexistence of prolate and oblate shapes is explained by calculating spectroscopic  $Q$  moments of the first and second  $2^+$  states, which is examined by the constrained Hartree-Fock method. The changes of the first band crossing and the nuclear deformation depending on the neutron number are discussed.

PACS numbers: 21.10.-k, 21.60.Cs, 21.10.Hw, 21.10.Re

## I. INTRODUCTION

The Ge isotopes  $^{66}\text{Ge}$  and  $^{68}\text{Ge}$  have been studied intensively in experiments ([1, 2, 3, 4, 5, 6] for  $^{66}\text{Ge}$  and [7, 8, 9, 10, 11] for  $^{68}\text{Ge}$ ) and in theoretical investigations [6, 9, 11, 12, 13, 14, 15, 16, 17, 18] for many years. A thorough theoretical investigation was carried out by Petrovici et al. with the excited VAMPIR (variation after mean field projection in realistic model spaces) method for  $^{68}\text{Ge}$  [9, 13, 14, 15]. The recent development of experimental techniques has accomplished detailed measurements of  $^{66}\text{Ge}$  [6] and  $^{68}\text{Ge}$  [11]. The new data have found several bands with positive and negative parities up to high spins ( $J \leq 28$ ). A hot topic of the Ge isotopes has been the coexistence of oblate and prolate shapes [19, 20, 21] and possible  $\gamma$  softness [22, 23]. The calculations based on the deformed mean field approximation in Refs. [6, 21] predict oblate shapes for the low-lying ground-state bands of  $^{66}\text{Ge}$  and  $^{68}\text{Ge}$ , which corresponds with the prediction of the excited VAMPIR calculations for  $^{68}\text{Ge}$ . Other theoretical approaches [12, 16, 17, 18], however, do not necessarily provide the same explanation as the mean field picture. The detailed new data demand to make further theoretical investigations into the structure of not only the low-energy states but the high-spin states.

We carried out shell model calculations on a spherical basis for the  $^{64}\text{Ge}$  nucleus in a previous paper [24]. The calculations with the extended  $P + QQ$  Hamiltonian [25, 26] in the configuration space ( $2p_{3/2}$ ,  $1f_{5/2}$ ,  $2p_{1/2}$ ,  $1g_{9/2}$ ) successfully described characteristics of the structure of  $^{64}\text{Ge}$ . The shell model has advantages that the nuclear deformation is dynamically determined through nuclear interactions and wave-functions are strictly determined, which makes it possible to calculate various physical quantities and to discuss the structure of bands in detail. The shell model is expected to be fruitful for the investigation into the new data on  $^{66}\text{Ge}$  and  $^{68}\text{Ge}$ .

For  $^{64}\text{Ge}$ ,  $^{65}\text{Ge}$ ,  $^{66}\text{Ge}$ ,  $^{67}\text{Ge}$ ,  $^{68}\text{Ge}$  and  $^{70}\text{Ge}$ , we have carried out large-scale shell model calculations using the calculation code [27]. The calculations reproduce well experimentally observed energy levels and other properties of  $^{66}\text{Ge}$  and  $^{68}\text{Ge}$ . In a recent paper [28], we have reported an interesting feature on the structural change of the even- $J$  positive-parity yrast states, i.e., successive three bands with different types of particle alignments (including proton-neutron alignment) in the  $g_{9/2}$  orbit. We show, in this paper, that similar changes are caused by various types of particle alignments in the  $g_{9/2}$  orbit, also in the other sequences of positive-parity yrast states with odd  $J$  and negative-parity yrast states with even  $J$  and odd  $J$ . Spectroscopic  $Q$  moments calculated with the reliable wave-functions provide useful information about the shape coexistence and shape variation depending on the neutron number. In order to investigate the shape coexistence and  $\gamma$  softness further, we calculate the potential energy surface in the plane of the deformation parameter  $q$  and the angle  $\gamma$  using the constrained Hartree-Fock (CHF) method too.

Section II presents parameters of the extended  $P + QQ$  Hamiltonian determined for  $^{65,66,67,68}\text{Ge}$  and energy levels obtained. In section III, experimental graphs of spin versus angular frequency and electromagnetic transition probabilities  $B(E2)$  and  $B(M1)$  are compared with the shell model results. In section IV, various types of particle alignments are investigated in the four sequences of positive- and negative-parity yrast states with even  $J$  and odd  $J$ . We discuss the change of the first band crossing in the Ge and Zn isotopes in section V. Section VI investigates the shape coexistence and the shape variation. A summary is given in section VII.

## II. LEVEL SCHEMES

The extended  $P + QQ$  Hamiltonian is composed of the single-particle energies, monopole corrections,  $J = 0$  and  $J = 2$  isovector pairing forces, quadrupole-quadrupole ( $QQ$ ) force and octupole-octupole ( $OO$ ) force (see Refs. [25, 26] in detail):

$$\begin{aligned} H &= H_{\text{sp}} + H_{\text{mc}} + H_{P_0} + H_{P_2} + H_{QQ} + H_{OO} \\ &= \sum_{\alpha} \varepsilon_{\alpha} c_{\alpha}^{\dagger} c_{\alpha} + H_{\text{mc}} - \sum_{J=0,2} \frac{1}{2} g_J \sum_{M\kappa} P_{JM1\kappa}^{\dagger} P_{JM1\kappa} \\ &\quad - \frac{1}{2} \frac{\chi_2}{b^4} \sum_M : Q_{2M}^{\dagger} Q_{2M} : - \frac{1}{2} \frac{\chi_3}{b^6} \sum_M : O_{3M}^{\dagger} O_{3M} :, \end{aligned} \quad (1)$$

where the force strengths  $\chi_2$  and  $\chi_3$  are defined so as to have the dimension of energy by excluding the harmonic-oscillator range parameter  $b$ . In Ref. [24] for  $^{64}\text{Ge}$ , we employed the same single-particle energies as those in Ref. [29] which are extracted from the energy levels of  $^{57}\text{Ni}$  ( $\varepsilon_{g_{9/2}} - \varepsilon_{p_{3/2}} = 3.7$  MeV). However, the parameters cannot reproduce the relative energies of the positive- and negative-parity states in odd-mass Ge isotopes. We therefore lowered the  $g_{9/2}$  orbit toward the  $pf$  shell so that our shell model can reproduce experimental level schemes of odd-mass and even-mass Ge isotopes and also  $^{66}\text{As}$  as a whole. This was linked with the search for force strengths. We thus obtained the following set of param-

eters for the Ge isotopes. The single-particle energies are

$$\begin{aligned} \varepsilon_{p_{3/2}} &= 0.00, & \varepsilon_{f_{5/2}} &= 0.77, \\ \varepsilon_{p_{1/2}} &= 1.11, & \varepsilon_{g_{9/2}} &= 2.50 \quad \text{in MeV.} \end{aligned} \quad (2)$$

The value  $\varepsilon_{g_{9/2}} = 2.5$  MeV coincides with that of Ref. [30]. The single-particle energies are discussed in Ref. [31]. The force strengths determined for  $^{66}\text{Ge}$  are

$$\begin{aligned} g_0 &= 0.27(64/A), & g_2 &= 0.0, \\ \chi_2 &= 0.25(64/A)^{5/3}, & \chi_3 &= 0.05(64/A)^2 \quad \text{in MeV,} \end{aligned} \quad (3)$$

with  $A = 66$ . We can get good results for  $^{68}\text{Ge}$  using the force strengths (3) with  $A = 68$ . However, a little better results are obtained by setting  $A = 66$  in Eq. (3) also for  $^{68}\text{Ge}$ . We therefore use the fixed force parameters (values of Eq. (3) with  $A = 66$ ) for the Ge isotopes in this paper. The adopted monopole corrections are:

$$\begin{aligned} H_{\text{mc}}^{T=1}(p_{3/2}, f_{5/2}) &= -0.3, & H_{\text{mc}}^{T=1}(p_{3/2}, p_{1/2}) &= -0.3, \\ H_{\text{mc}}^{T=1}(f_{5/2}, p_{1/2}) &= -0.4, & H_{\text{mc}}^{T=1}(g_{9/2}, g_{9/2}) &= -0.2, \\ H_{\text{mc}}^{T=0}(g_{9/2}, g_{9/2}) &= -0.1 \quad \text{in MeV.} \end{aligned} \quad (4)$$

Let us show energy levels of  $^{66}\text{Ge}$  and  $^{68}\text{Ge}$  calculated with the parameters (2), (3) and (4), in Figs. 1 and 2. In these figures, the calculated results excellently explain the energy levels observed in  $^{66}\text{Ge}$  and  $^{68}\text{Ge}$  [6, 11], reproducing several sequences of the positive- and negative-parity states (except for a superdeformed band of  $^{68}\text{Ge}$  which is not shown in Fig. 2). For  $^{68}\text{Ge}$ , detailed band scheme was proposed from  $\Delta J = 2$  electromagnetic transitions in the experiment [11], where, for instance, the  $14_4^+$  and  $16_6^+$  states are connected to the yrast states  $8_1^+$ ,  $10_1^+$  and  $12_1^+$ . This sequence of the states is shown in the most left columns of the experimental and calculated results respectively in Fig. 2. The calculated  $14_3^+$  and  $16_4^+$  states which are connected by large  $B(E2)$  values to the yrast  $12_1^+$  state correspond well to the experimental  $14_4^+$  and  $16_6^+$  states as shown in Fig. 2. (Note that there are many levels with  $J^{\pi} = 14^+$  ( $J^{\pi} = 16^+$ ) near  $14_3^+$  ( $16_4^+$ ) in the calculation.) We calculated also energy levels of  $^{64}\text{Ge}$  and  $^{70}\text{Ge}$ , although high-spin states with  $J^{\pi} \geq 10^+$  have not been detected. Our model approximately reproduces the experimental energy levels up to  $8^+$  in  $^{64}\text{Ge}$  and  $^{70}\text{Ge}$ , as shown in Fig. 14 later.

The extended  $P + QQ$  model with the above parameters describes quite well experimental energy levels of the odd-mass isotopes  $^{65}\text{Ge}$  and  $^{67}\text{Ge}$  [32], as shown in Fig. 3. The energy levels of the positive- and negative-parity states are approximately reproduced, although the agreement with experimental ones in the odd-mass Ge isotopes is worse than that in the even-mass Ge isotopes. There are contradictions between theory and experiment in the order of some energy levels with serial spins, and the calculated high-spin states are pushed up as compared with the experimental ones. However, our model correctly predicts the spins of the ground states,  $3/2^-$  for  $^{65}\text{Ge}$  and

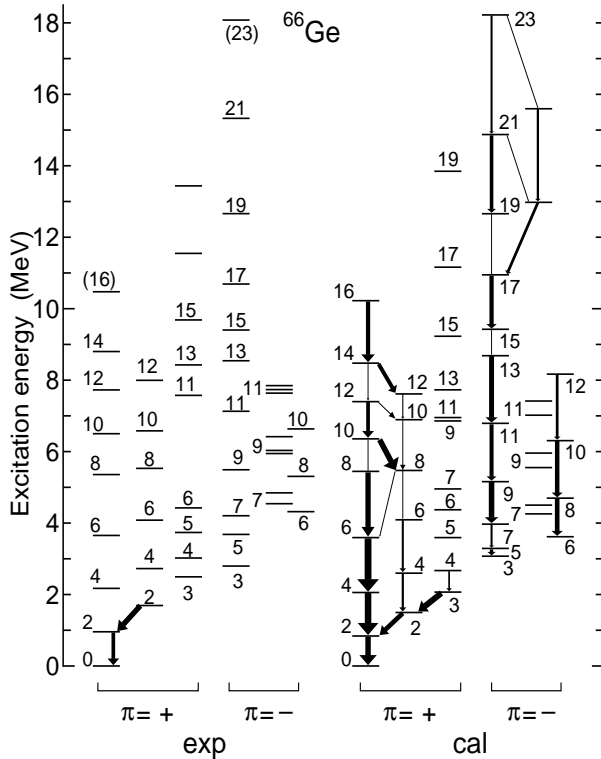


FIG. 1: Experimental and calculated energy levels of  $^{66}\text{Ge}$ . The widths of the arrows denote relative values of  $B(E2)$ .

$1/2^-$  for  $^{67}\text{Ge}$ . We can see one-to-one correspondence between the experimental and calculated energy levels of  $^{65}\text{Ge}$  and  $^{67}\text{Ge}$  in Fig. 3. Such a consistent description of both the even- and odd-mass Ge isotopes has not been reported.

From these results, the extended  $P + QQ$  interaction can be regarded as an almost realistic effective interaction for the Ge isotopes. The success in reproducing the level schemes testifies to the reliability of the wave-functions obtained. We shall calculate various quantities using the obtained wave-functions and discuss the structure of  $^{66}\text{Ge}$  and  $^{68}\text{Ge}$  in the following sections.

### III. MOMENTS OF INERTIA AND ELECTROMAGNETIC TRANSITIONS

#### A. $J - \omega$ graphs

Illustrating the relation between the spin  $J$  and the rotational frequency  $\omega(J) = (E(J) - E(J-2))/2$  with a graph (which we call “ $J - \omega$  graph”) is useful in seeing the change of nuclear structure, because the moment of in-

ertia  $J/\omega(J)$  reflects competition among various nuclear correlations.

Figure 4(a) shows the  $J - \omega$  graphs for the three sequences of positive-parity states of  $^{66}\text{Ge}$  which are illustrated in Fig. 1: the even- $J$  yrast states including the ground-state ( $gs$ ) band up to  $8_1^+$ ; the second band on the  $2_2^+$  state; the odd- $J$  yrast states on the  $11_1^+$  state. Our model reproduces well the changes of the moments of inertia for these three sequences of positive-parity states. The agreement with the experimental moments of inertia is much better than that of the total Routhian surface (TRS) calculations [6] and that of the projected shell model [31]. This indicates that our wave-functions are better than those of the TRS calculations.

In Fig. 4(a), the  $J - \omega$  graph for the even- $J$  positive-parity yrast states displays a stable (collective) rotation up to  $8_1^+$  and a sharp backbending toward  $10_1^+$ . The remarkable backbending from  $8_1^+$  to  $10_1^+$  indicates a structural change. We shall focus our attention on this phenomenon later. The straight line starting from  $14_1^+$  after the transitional state  $12_1^+$  is notable in the  $J - \omega$  graph for the even- $J$  yrast states in Fig. 4(a). It is also interesting that the  $J - \omega$  graph for the odd- $J$  states  $13_1^+$ ,  $15_1^+$ ,  $17_1^+$  and  $19_1^+$  is almost equal to the  $J - \omega$  graph for the even- $J$  states  $14_1^+$ ,  $16_1^+$  and  $18_1^+$ . The similar straight lines suggest that these states are generated by the same rotor and the structure varies gradually. The  $J - \omega$  graphs in Fig. 4(a) predict structural changes at  $20_1^+$  in the sequence of

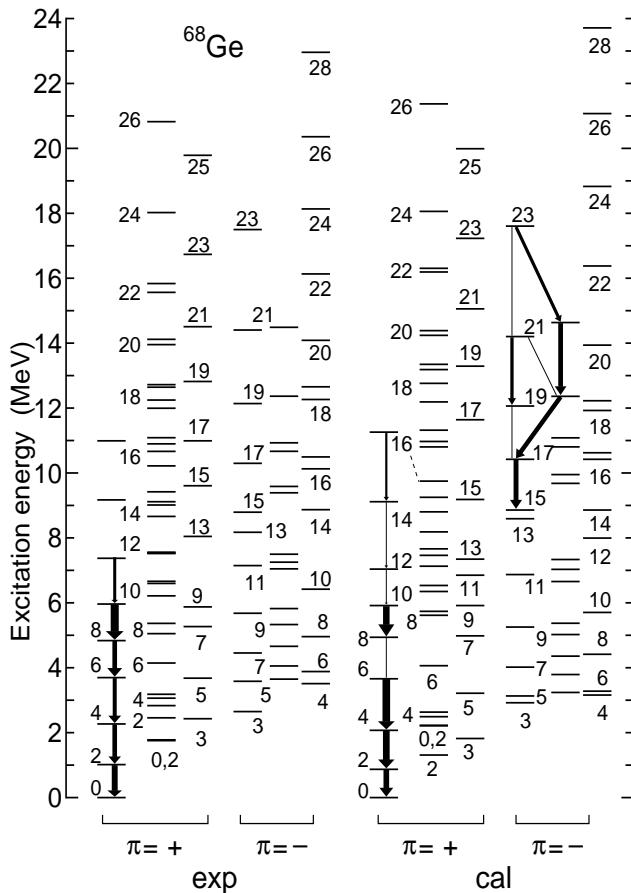


FIG. 2: Experimental and calculated energy levels of  $^{68}\text{Ge}$ . The widths of the arrows denote relative values of  $B(E2)$ .

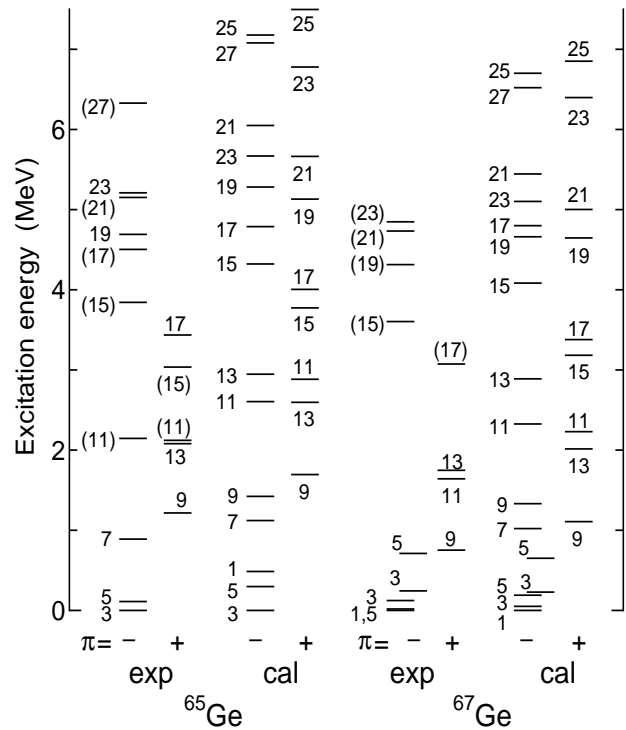


FIG. 3: Experimental and calculated energy levels of  $^{65}\text{Ge}$  and  $^{67}\text{Ge}$ . The spin of each state is denoted by the double number  $2J$ .

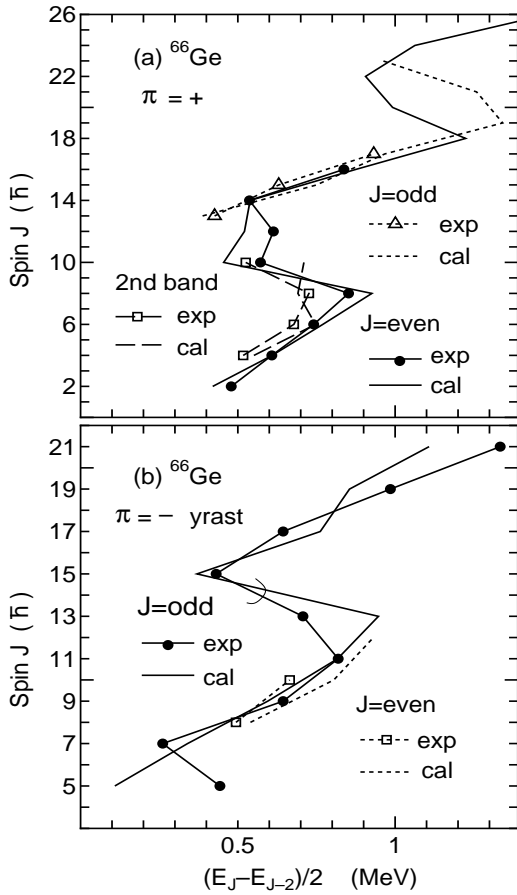


FIG. 4: The  $J - \omega$  graphs for  $^{66}\text{Ge}$ : (a) the positive-parity yrast states with even  $J$  and odd  $J$ , and the second band on  $2_2^+$ ; (b) the negative-parity yrast states with even  $J$  and odd  $J$ .

the even- $J$  positive-parity yrast states and at  $21_1^+$  in the sequence of the odd- $J$  positive-parity yrast states.

Figure 4(b) shows the  $J - \omega$  graphs for the negative-parity yrast states with odd  $J$  and even  $J$  of  $^{66}\text{Ge}$ . Our model reproduces well the change of the experimental moments of inertia. For the odd- $J$  yrast states, although there are deviations from the experimental graph at  $5_1^-$  and  $13_1^-$ , the sharp backbending toward  $15_1^-$  is well explained. This backbending indicates a structural change at the  $15_1^-$  state in the sequence of the odd- $J$  negative-parity yrast states. The  $J - \omega$  graph for the odd- $J$  yrast states has a straight line for the  $15_1^-$ ,  $17_1^-$ ,  $19_1^-$  and  $21_1^-$  states, which is nearly equal to the two lines for the even- $J$  positive-parity yrast states ( $14_1^+$ ,  $16_1^+$ ,  $18_1^+$ ) and for the odd- $J$  ones ( $13_1^+$ ,  $15_1^+$ ,  $17_1^+$ ,  $19_1^+$ ) in Fig. 4(a). These three bands ( $15_1^- - 21_1^-$ ,  $14_1^+ - 18_1^+$  and  $13_1^+ - 19_1^+$ ) seem to have a similar structure. Figure 4(b) also shows that the even- $J$  states  $6_1^-$ ,  $8_1^-$  and  $10_1^-$  have a similar structure to the odd- $J$  states  $7_1^-$ ,  $9_1^-$  and  $11_1^-$ .

We show the  $J - \omega$  graphs for the positive-parity yrast states with even  $J$  and odd  $J$  of  $^{68}\text{Ge}$ , in Fig. 5(a). Here we illustrate the  $J - \omega$  graphs for the yrast states instead

of the sequence connected by  $\Delta J = 2$  transitions (which is shown in the most left columns of the experimental and calculated energy levels in Fig. 2), because we are concerned with how the structure changes as the spin  $J$  increases and wish to compare the  $^{68}\text{Ge}$  graphs with the  $^{66}\text{Ge}$  graphs.

In Fig. 5(a), our model reproduces quite well the experimental  $J - \omega$  graphs for  $^{68}\text{Ge}$ , except for  $18_1^+$  and  $17_1^+$ . The comparison between Figs. 4(a) and 5(a) indicates a similarity between the low-spin states up to  $6_1^+$  of  $^{66}\text{Ge}$  and  $^{68}\text{Ge}$  in the moments of inertia (hence the structure). There is, however, a significant difference between  $^{66}\text{Ge}$  and  $^{68}\text{Ge}$ . The backbending takes place at  $8_1^+$  in  $^{68}\text{Ge}$ , while it happens at  $10_1^+$  in  $^{66}\text{Ge}$ . This difference is another interest discussed later. The theoretical  $J - \omega$  graph for the states  $14_1^+$ ,  $16_1^+$  and  $18_1^+$  of  $^{68}\text{Ge}$  is similar to the graph for the corresponding states of  $^{66}\text{Ge}$ . The experimental  $J - \omega$  graph is different from the theoretical one at  $18_1^+$  in  $^{68}\text{Ge}$ . The experiment [11] observed a few sets of  $14^+$ ,  $16^+$ ,  $18^+$  and  $20^+$  belonging to different bands. The above discrepancy in the energy spacing  $E(18_1^+) - E(16_1^+)$  in Fig. 5(a) suggests a considerable interplay between these bands near  $16^+$  and  $18^+$  which

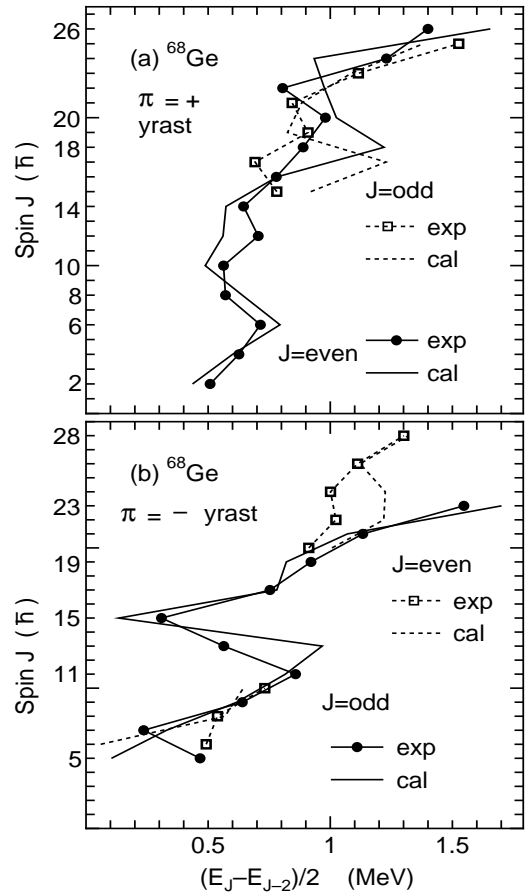


FIG. 5: The  $J - \omega$  graphs for  $^{68}\text{Ge}$ : (a) the positive-parity yrast states with even  $J$  and odd  $J$ ; (b) the negative-parity yrast states with even  $J$  and odd  $J$ .

is not sufficiently taken into account in our model. The two  $J-\omega$  graphs for the experimental even- $J$  yrast states on  $18_1^+$  and odd- $J$  yrast states on  $17_1^+$ , which suggest a resemblance between them, are well reproduced by the theory.

The  $J-\omega$  graphs for the negative-parity yrast states with odd  $J$  and even  $J$  of  $^{68}\text{Ge}$  are illustrated in Fig. 5(b). Our model is successful in describing the change of the moments of inertia for the odd- $J$  yrast states, except for  $5_1^-$  and  $13_1^-$ . The sharp backbending toward  $15_1^-$  is finely reproduced. The low-spin band from  $5_1^-$  to  $11_1^-$  (except for the bad energy spacing between  $3_1^-$  and  $5_1^-$ ) and the high-spin sequence on  $15_1^-$  are also reproduced well. It is notable that the  $J-\omega$  graph for the odd- $J$  negative-parity yrast states of  $^{68}\text{Ge}$  resembles that of  $^{66}\text{Ge}$ , which suggests a similar structure of these states in  $^{68}\text{Ge}$  and  $^{66}\text{Ge}$ . In  $^{68}\text{Ge}$ , high-spin negative-parity yrast states with even  $J$  are experimentally observed up to  $28_1^-$  [11]. The moments of inertia of these states are well reproduced by the theory, in Fig. 5(b).

### B. $B(E2)$ and $B(M1)$

To investigate the correspondence between experimental and calculated bands, we calculated reduced  $E2$  transition probabilities using the effective charge  $e_p = 1.5e$  for proton and  $e_n = 0.5e$  for neutron, and the harmonic-oscillator range parameter  $b = A^{1/3}$ . Experimental  $B(E2)$  values and some of the calculated  $B(E2)$  values are denoted by the widths of the arrows in Figs. 1 and 2, and are tabulated in Table I, where the experimental data are taken from the evaluated nuclear structure data file [32].

There are not sufficient data on  $B(E2)$  for  $^{66}\text{Ge}$ . The experimental large value of  $B(E2 : 2_2^+ \rightarrow 2_1^+)$  and small value of  $B(E2 : 2_2^+ \rightarrow 0_1^+)$  are well reproduced by the calculations. Although the calculated value  $281 e^2\text{fm}^4$  of  $B(E2 : 2_1^+ \rightarrow 0_1^+)$  is larger than the experimental one  $190 \pm 36 e^2\text{fm}^4$ , the qualitative trend of the observed  $\Delta J = 2$  transitions [6] in the two cascade bands (the  $gs$  band and the second positive-parity band on  $2_2^+$ ) up to  $J = 8$  can be explained by the calculated  $B(E2)$  values. The large ratio of  $B(E2 : 2_2^+ \rightarrow 2_1^+)/B(E2 : 2_2^+ \rightarrow 0_1^+)$  was discussed as a signature of the triaxiality of  $^{64}\text{Ge}$  in Ref. [24]. The experimental and calculated ratios suggest the same nature of  $^{66}\text{Ge}$  as that of  $^{64}\text{Ge}$ , which is consistent with the previous understanding [6] of the  $\gamma$  softness. There are similarities between  $^{66}\text{Ge}$  and  $^{64}\text{Ge}$  with respect to other  $B(E2)$  values calculated with the parameters (2), (3) and (4). We can presume a similar structure in the low-spin states before the backbending in  $^{66}\text{Ge}$  and  $^{64}\text{Ge}$ .

It is notable in the calculated results for  $^{66}\text{Ge}$  that  $B(E2 : 10_1^+ \rightarrow 8_1^+)$  is small in correspondence to the backbending at  $10_1^+$  seen in Fig. 4(a). This shows that the structure of the yrast states changes at  $10_1^+$  in  $^{66}\text{Ge}$ . The larger  $B(E2 : 10_1^+ \rightarrow 8_2^+)$  value than  $B(E2 : 10_1^+ \rightarrow$

$8_1^+)$  in the calculation (probably in experiment) shows the continuation of the  $10_1^+$  state to the  $8_2^+$  state. These results indicate a band crossing between  $J = 8$  and  $J = 10$ . The  $10_2^+$  state is, however, not connected to the  $8_1^+$  state, because  $B(E2 : 10_2^+ \rightarrow 8_1^+)$  is small in theory. The experimentally observed inter-band transition  $8_2^+ \rightarrow 8_1^+$  suggests significant mixing of  $8^+$  states. Above  $10_1^+$ , the calculated  $B(E2 : J_1^+ \rightarrow (J-2)_1^+)$  values between the yrast states become quite large up to  $18_1^+$ , except that  $B(E2 : 14_1^+ \rightarrow 12_1^+)$  is small. This explains the cascade of  $\Delta J = 2$  transitions from the tentative  $16^+$  state observed in Ref. [6]. The small value of  $B(E2 : 14_1^+ \rightarrow 12_1^+)$  corresponds to the structural change at  $14_1^+$  suggested by the  $J-\omega$  graph in Fig. 4(a). Our model predicts another interesting backbending at  $11_1^+$  in the sequence of the odd- $J$  positive-parity yrast states. As shown in Table II, the calculated  $B(E2 : 11_1^+ \rightarrow 9_1^+)$  value is very small, while  $B(E2 : \Delta J = 2)$  is large below  $9_1^+$  and above  $11_1^+$ . This shows that the structure changes at the  $11_1^+$  state. In other words, the sequence of the odd- $J$  positive-parity yrast states is composed of two bands, from  $3_1^+$  till  $9_1^+$  and from  $11_1^+$  to  $19^+$ . Also for the sequence of the odd- $J$  negative-parity yrast states of  $^{66}\text{Ge}$ , the  $B(E2 : 15_1^- \rightarrow 13_1^-)$  value is very small, which corresponds to the backbending at  $15_1^-$  both in the experimental and calculated  $J-\omega$  graphs shown in Fig. 4(b).

The new experiment for  $^{66}\text{Ge}$  [6] found a cascade of  $\Delta J = 1$  transitions connecting two  $\Delta J = 2$  sequences with even  $J$  and odd  $J$  ( $15_1^+ \rightarrow 14_1^+$  and  $13_1^+ \rightarrow 12_1^+ \rightarrow 11_1^+ \rightarrow 10_1^+$ ), and supposed that the  $\Delta J = 1$  transitions are  $M1$  transitions. We calculated both of  $B(E2)$

TABLE I:  $B(E2)$  values for the positive-parity yrast states and some collective states of  $^{66}\text{Ge}$  and  $^{68}\text{Ge}$ . Non-yrast states are distinguished with their subscripts from the yrast states with no subscript. The subscript denotes a serial number for each spin  $J$ . The most right column shows the  $B(E2)$  values of Ref. [15].

$J_i^+ \rightarrow J_f^+$	$^{66}\text{Ge} [e^2\text{fm}^4]$		$^{68}\text{Ge} [e^2\text{fm}^4]$		
	exp	cal	exp	cal	[15]
$2 \rightarrow 0$	$190 \pm 36$	281	$292 \pm 33$	278	100
$4 \rightarrow 2$	$>152$	337	$229 \pm 30$	330	563
$6 \rightarrow 4$	$>19$	351	$198 \pm 66$	376	792
$8 \rightarrow 6$		275	$231 \pm 49$	0.09	291
$8_2 \rightarrow 6$		4	$198_{-198}^{+66}$		321
$8 \rightarrow 6_2$		4	$157 \pm 33$		0.02
$8_2 \rightarrow 6_2$		0.05	$297_{-297}^{+99}$		3.8
$10 \rightarrow 8$	$<74$	5	$396_{-396}^{+82}$		852
$10_2 \rightarrow 8$		1.8	$>25$		2.7
$10 \rightarrow 8_2$	$<206$	285			0.01
$10_2 \rightarrow 8_2$		33	$>308$		0.25
$12 \rightarrow 10$		191	$148_{-148}^{+66}$	49	853
$14 \rightarrow 12$		16		70	273
$14_3 \rightarrow 12$		32		42	
$16 \rightarrow 14$		219		199	672
$16_4 \rightarrow 14_3$		151		107	
$2_2 \rightarrow 0$	$1.6 \pm 0.6$	4	$2.3 \pm 0.4$	0.5	
$2_2 \rightarrow 2$	$269 \pm 127$	233	$8.0 \pm 3.5$	375	

and  $B(M1)$  to examine this supposition. The results are shown in Table II. The  $B(M1)$  values obtained with our model are consistent with the results of Ref. [6] that  $B(M1 : 12_1^+ \rightarrow 11_1^+)$  is large, and  $B(M1 : 13_1^+ \rightarrow 12_1^+)$  and  $B(M1 : 15_1^+ \rightarrow 14_1^+)$  is small. However, the  $B(M1 : 14_1^+ \rightarrow 13_1^+)$  value is small in contrast to the predicted staggering. The experimental value of  $B(M1 : 2_2^+ \rightarrow 2_1^+)$  is  $0.008 \mu_N^2$  and the calculated one is  $0.0023 \mu_N^2$ . The roughly good prediction testifies to a considerable reliability of our  $B(M1)$  values. Table II shows that the  $B(E2 : \Delta J = 1)$  values are not negligible for the states  $10_1^+$  to  $15_1^+$ , which suggests possible mixing of  $E2$  and  $M1$  transitions.

For  $^{68}\text{Ge}$ , experimental  $B(E2)$  values of the  $gs$  band up to  $6_1^+$  are better reproduced by the present shell model calculation as compared with the VAMPIR calculation as shown in Table II. Except for several band crossings, our model successfully predicts large  $E2$  transitions in the four sequences of the positive- and negative-parity states with even  $J$  and odd  $J$  deduced by cascades of  $\Delta J = 2$  transitions in Ref. [11]. Some of the calculated  $B(E2)$  values for  $8^+ \rightarrow 6^+$  transitions do not correspond with the experimental values. The small value of  $B(E2 : 8_1^+ \rightarrow 6_1^+)$  is notable in the calculated result. This is in agreement with the backbending at  $8_1^+$  in Fig. 5(a), which suggests that a structural change takes place at the  $8_1^+$  state in  $^{68}\text{Ge}$ , in contrast to the backbending at  $10_1^+$  and the small value of  $B(E2 : 10_1^+ \rightarrow 8_1^+)$  in  $^{66}\text{Ge}$ . The calculation predicts a large value for  $B(E2 : 8_2^+ \rightarrow 6_1^+)$ , suggesting that the  $gs$  band up to  $6_1^+$  is connected to the  $8_2^+$  state, and a band crossing happens between  $J = 6$  and  $J = 8$ . This is consistent with the result of the VAMPIR calculation, but contradicts the result of the particle-rotor model [8] in which the  $8_3^+$  state is identified as the continuation of the  $gs$  band. We note again that the sequence of the states ( $8_1^+, 10_1^+, 12_1^+, 14_4^+, 16_6^+$ ) connected by strong  $E2$  transitions in experiment cor-

responds well with the sequence of the states ( $8_1^+, 10_1^+, 12_1^+, 14_3^+, 16_4^+$ ) connected by large  $B(E2)$  values in theory. To other bands assigned in the experiment [11], our model has corresponding states connected by large  $B(E2)$  values except that  $B(E2)$  values become small at band crossings.

The  $11_1^+$  state has not experimentally been observed in the sequence of the odd- $J$  positive-parity yrast states of  $^{68}\text{Ge}$ . Our model provides very small values for  $B(E2 : 11_1^+ \rightarrow 9_1^+)$  and  $B(E2 : 9_1^+ \rightarrow 7_1^+)$ , which suggests a structural change near the  $9_1^+$  and  $11_1^+$  states. The situation is rather complicated as compared with the backbending in other bands. In order to compare the  $M1$  transitions between the states from  $J = 10$  to  $J = 15$  in  $^{68}\text{Ge}$  with those in  $^{66}\text{Ge}$ , we calculated  $B(M1)$  and  $B(E2)$  values also for  $^{68}\text{Ge}$ . Table II shows that the calculated  $B(M1)$  values for these states of  $^{68}\text{Ge}$  are, up to  $14^+$ , similar to those of  $^{66}\text{Ge}$  but  $B(M1 : 15_1^+ \rightarrow 14_1^+)$  is large in  $^{68}\text{Ge}$  in contrast to  $^{66}\text{Ge}$ . For these states, the  $B(E2 : \Delta J = 1)$  values are a little smaller in  $^{68}\text{Ge}$  than in  $^{66}\text{Ge}$ . Our model suggests that the  $M1$  transition could contribute to the  $\Delta J = 1$  transitions also in  $^{68}\text{Ge}$ .

For  $^{68}\text{Ge}$ , the continuation of the negative-parity states  $17_1^-, 19_1^-, 21_1^-$  and  $23_1^-$  and the termination of the odd- $J$  negative-parity band are discussed in Ref. [11]. The present shell model, which reproduces well these experimental energy levels as shown in Fig. 2, yields the following  $B(E2)$  values: 156, 234, 218 and 243 in  $e^2\text{fm}^4$  for the transitions  $23_1^- \rightarrow 21_2^- \rightarrow 19_2^- \rightarrow 17_1^- \rightarrow 15_1^-$ ; 0.1, 163 and 9 in  $e^2\text{fm}^4$  for the transitions  $23_1^- \rightarrow 21_1^- \rightarrow 19_1^- \rightarrow 17_1^-$ . These  $B(E2)$  values indicate the continuation of the states  $17_1^-, 19_2^-$  and  $23_1^-$ . This result disagrees with the considerations in Ref. [11], where the  $17_1^-$  state is considered to be a possible terminating state. Also in  $^{66}\text{Ge}$ , as shown in Fig. 1, the calculated  $B(E2)$  values suggest the continuation of the states  $17_1^-, 19_2^-$  and  $21_2^-$ . The calculations, however, show a difference between  $^{68}\text{Ge}$  and  $^{66}\text{Ge}$ , i.e.,  $B(E2 : 23_1^+ \rightarrow 21_2^+)$  is very small as compared with  $B(E2 : 23_1^+ \rightarrow 21_1^+)$  in  $^{66}\text{Ge}$  in opposition to  $^{68}\text{Ge}$ . This remains as a question about the band on  $15_1^-$  in  $^{66}\text{Ge}$ .

TABLE II: Calculated  $B(E2)$  ( $e^2\text{fm}^4$ ) and  $B(M1)$  ( $\mu_N^2$ ) values for the positive-parity states from  $J = 9$  to  $J = 15$  of  $^{66}\text{Ge}$  and  $^{68}\text{Ge}$ . Non-yrast states are distinguished with their subscripts from the yrast states with no subscript.

$J_i^+ \rightarrow J_f^+$	$^{66}\text{Ge}$ cal		$^{68}\text{Ge}$ cal	
	$B(E2)$	$B(M1)$	$B(E2)$	$B(M1)$
$11 \rightarrow 9$	0.14		1.2	
$11 \rightarrow 10$	11	0.036	7	0.001
$11 \rightarrow 10_2$	16	0.26	22	0.33
$12 \rightarrow 10$	191		49	
$12 \rightarrow 11$	22	0.66	0.5	0.14
$13 \rightarrow 11$	312		180	
$13 \rightarrow 12$	17	0.021	19	0.030
$14 \rightarrow 12$	16		70	
$14 \rightarrow 13$	23	0.003	9	0.043
$14_3 \rightarrow 13$	0.4		0.02	0.044
$15 \rightarrow 13$	270		166	
$15 \rightarrow 14$	3	0.015	4	0.20
$15 \rightarrow 14_3$	12		6	0.048

We have seen backbending at  $15_1^-$  in the sequence of the odd- $J$  negative-parity yrast states of  $^{68}\text{Ge}$  both in experiment and theory, in Fig. 5(b). The small value of  $B(E2 : 15_1^- \rightarrow 13_1^-)$  indicates a change in the structure of this sequence of states. The backbending at  $15_1^-$  corresponds to that in  $^{66}\text{Ge}$ . The calculated result in Fig. 2 shows a sign of backbending at  $14_1^-$  in the even- $J$  negative-parity yrast states. However, the small values of  $B(E2 : 14_1^- \rightarrow 12_1^-)$  and  $B(E2 : 12_1^- \rightarrow 10_1^-)$  suggest a complicated structural change near the  $12_1^-$  and  $14_1^-$  states which is similar to that of the odd- $J$  positive-parity yrast states. The complicated situations may be related to the missing of  $12_1^-$  and  $11_1^+$  in the experiment [11].

## IV. PARTICLE ALIGNMENTS

### A. Particle alignments in the even- $J$ positive-parity yrast states

We calculated expectation values of proton and neutron numbers in each orbit ( $\langle n_a^\pi \rangle$  and  $\langle n_a^\nu \rangle$ ) and the spectroscopic  $Q$  moment, in order to investigate the structure of  $^{66}\text{Ge}$  and  $^{68}\text{Ge}$ . The calculated results for the even- $J$  positive-parity yrast states and some other states of  $^{66}\text{Ge}$  are shown in Table III. We have shown in a recent paper [28] that the structural changes revealed in the  $J - \omega$  graph of Fig. 4(a) can be explained by successive alignments of three combinations of nucleons in the  $g_{9/2}$  orbit: two-neutron ( $2n$ ) alignment coupled to  $T = 1$ ,  $J = 8$ ; one-proton-one-neutron ( $1p1n$ ) alignment coupled to  $T = 0$ ,  $J = 9$ ; two-proton-two-neutron ( $2p2n$ ) alignment coupled to  $T = 0$ ,  $J = 16$ , i.e.,  $[(g_{9/2}^\pi)_{T=1, J=8}^2 (g_{9/2}^\nu)_{T=1, J=8}^2]_{T=0, J=16}$ . The scenario of the changes is as follows: (a) The  $2n$  alignment takes place at the  $8_2^+$  state. The  $2n$  aligned band crosses the  $gs$  band between  $J = 8$  and  $J = 10$ . (b) The  $1p1n$  aligned band competes with the  $2n$  aligned band near  $J = 10$  and  $J = 12$ , and there is interplay between the two bands. (c) The  $1p1n$  alignment overwhelms the  $2n$  alignment at  $14_1^+$ , and the  $1p1n$  aligned band appears in the yrast line from  $14_1^+$  to  $18_1^+$ . (d) The  $2p2n$  aligned band takes over

TABLE III: Expectation values of proton and neutron numbers in the four orbits, calculated for the even- $J$  positive-parity yrast states and some low-energy states of  $^{66}\text{Ge}$ . Calculated  $Q$  moments (in  $e \text{ fm}^2$ ) are also tabulated.

$^{66}\text{Ge}$	proton				neutron				$Q$
	$p_{3/2}$	$f_{5/2}$	$p_{1/2}$	$g_{9/2}$	$p_{3/2}$	$f_{5/2}$	$p_{1/2}$	$g_{9/2}$	
$0_1^+$	1.72	1.72	0.50	0.06	2.42	2.68	0.77	0.13	
$2_1^+$	1.71	1.70	0.53	0.06	2.40	2.77	0.70	0.13	-23.2
$4_1^+$	1.72	1.72	0.49	0.07	2.39	2.82	0.67	0.12	-27.9
$6_1^+$	1.71	1.79	0.43	0.07	2.35	2.83	0.70	0.12	-35.8
$8_1^+$	1.67	1.84	0.42	0.08	2.42	2.67	0.74	0.16	-39.4
$8_2^+$	1.60	1.72	0.51	0.18	1.62	1.88	0.61	1.89	-59.9
$10_1^+$	1.45	1.49	0.63	0.43	1.75	1.95	0.61	1.69	-70.8
$12_4^+$	1.52	1.53	0.54	0.41	1.69	2.02	0.61	1.67	-58.5
$10_4^+$	1.19	1.20	0.64	0.98	1.78	2.20	0.94	1.08	-80.2
$12_2^+$	1.30	1.17	0.61	0.93	2.05	2.16	0.59	1.20	-80.5
$14_1^+$	1.29	1.17	0.54	1.00	1.97	2.12	0.85	1.06	-83.7
$16_1^+$	1.28	1.15	0.57	1.00	1.88	2.38	0.66	1.08	-80.5
$18_1^+$	1.26	1.17	0.55	1.02	1.84	2.45	0.63	1.07	-81.8
$18_2^+$	0.64	0.76	0.61	1.99	1.59	1.78	0.61	2.03	-83.9
$20_1^+$	0.73	0.84	0.48	1.95	1.55	1.73	0.64	2.07	-84.7
$22_1^+$	0.69	0.84	0.46	2.00	1.38	2.02	0.59	2.01	-82.9
$24_1^+$	0.78	1.03	0.19	2.00	1.38	2.07	0.54	2.01	-84.7
$26_1^+$	0.91	1.09	0.00	2.01	1.32	2.09	0.58	2.02	-86.1
$2_2^+$	1.69	1.75	0.48	0.09	2.38	2.55	0.93	0.14	+20.9
$4_2^+$	1.75	1.61	0.57	0.08	2.40	2.78	0.68	0.14	-20.6
$6_2^+$	1.70	1.70	0.52	0.09	2.48	2.72	0.68	0.14	-16.5
$3_1^+$	1.79	1.56	0.56	0.10	2.44	2.72	0.70	0.14	-0.9
$4_3^+$	1.69	1.62	0.60	0.09	2.50	2.69	0.67	0.14	+5.6

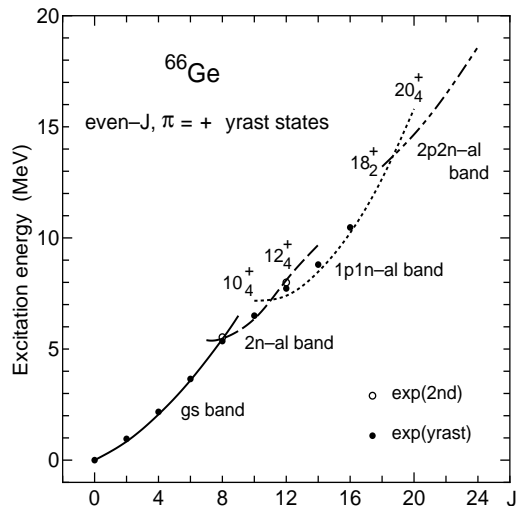


FIG. 6: Comparison of the calculated four bands (curves) with the experimental yrast states (solid circles) for  $^{66}\text{Ge}$ .

as the yrast state at  $20_1^+$ , continuing up to the  $26_1^+$  state where the band terminates. This scenario is narrated by the variation of the proton and neutron numbers listed in Table III. The successive alternations of the four bands cause the changes of the  $B(E2)$  values at the band crossings, as shown in section III. The abrupt change of the spectroscopic  $Q$  moment from  $8_1^+$  to  $10_1^+$  also testifies to the band crossing. We illustrate the successive four bands with a graph of the excitation energy versus the spin  $J$  (we call it “ $E_x - J$  graph”), in Fig. 6. Here, the  $10_4^+$  state has a dominant component of the aligned  $1p1n$  pair in the  $g_{9/2}$  orbit, the  $12_4^+$  state has a dominant component of the aligned  $2n$  pair in the  $g_{9/2}$  orbit, and the  $18_2^+$  state belongs to the  $2p2n$  aligned band.

Let us show the results for the even- $J$  positive-parity yrast states of  $^{68}\text{Ge}$ , instead of repeating the results for  $^{66}\text{Ge}$  shown in Ref. [28]. Table IV lists the proton and neutron numbers  $\langle n_a^\pi \rangle$  and  $\langle n_a^\nu \rangle$  for the even- $J$  positive-parity yrast states and some other states of  $^{68}\text{Ge}$ . This table shows that the structural changes parallel to those mentioned above for  $^{66}\text{Ge}$  happen in  $^{68}\text{Ge}$ . A remarkable difference of  $^{68}\text{Ge}$  from  $^{66}\text{Ge}$  is the  $2n$  alignment at the  $8_1^+$  state of  $^{68}\text{Ge}$ , where the neutron number  $\langle n_{g_{9/2}}^\nu \rangle \approx 2$  indicates the  $2n$  alignment in the  $g_{9/2}$  orbit. We illustrate the changes of  $\langle n_{g_{9/2}}^\pi \rangle$  and  $\langle n_{g_{9/2}}^\nu \rangle$  in Fig. 7, and expectation values of the spin and isospin of nucleons in the  $g_{9/2}$  orbit (which are denoted by  $J_{g_{9/2}}$  and  $T_{g_{9/2}}$ ) in Fig. 8. Here, we evaluate the spin  $J_{g_{9/2}}$  and the isospin  $T_{g_{9/2}}$  as follows:  $J_{g_{9/2}} = [(\langle \hat{J}_{g_{9/2}} \rangle^2) + 1/4]^{1/2} - 1/2$  and  $T_{g_{9/2}} = [(\langle \hat{t}_{g_{9/2}} \rangle^2) + 1/4]^{1/2} - 1/2$ . Figures 7 and 8 narrate the same scenario as that mentioned above for  $^{66}\text{Ge}$ .

In  $^{68}\text{Ge}$ , while the  $gs$  band continues to the  $8_2^+$  state, the  $2n$  aligned band crosses the  $gs$  band before  $J = 8$ . The abrupt change of the  $Q$  moment at  $8_1^+$  indicates the band crossing. The yrast states  $8_1^+$  and  $10_1^+$  are members of the  $2n$  aligned band. Passing the transitional

TABLE IV: Expectation values of proton and neutron numbers in the four orbits, calculated for the even- $J$  positive-parity yrast states and some low-energy states of  $^{68}\text{Ge}$ . Calculated  $Q$  moments (in  $e \text{ fm}^2$ ) are also tabulated.

$^{68}\text{Ge}$	proton				neutron				$Q$
	$p_{3/2}$	$f_{5/2}$	$p_{1/2}$	$g_{9/2}$	$p_{3/2}$	$f_{5/2}$	$p_{1/2}$	$g_{9/2}$	
$0_1^+$	1.74	1.69	0.51	0.07	3.05	3.50	1.21	0.24	
$2_1^+$	1.72	1.69	0.51	0.08	3.02	3.51	1.24	0.23	-6.8
$4_1^+$	1.75	1.70	0.46	0.09	3.02	3.46	1.31	0.22	-8.1
$6_1^+$	1.76	1.73	0.40	0.11	3.02	3.39	1.37	0.22	-13.3
$8_2^+$	1.80	1.79	0.29	0.12	2.98	3.22	1.54	0.25	-13.2
$8_1^+$	1.66	1.72	0.50	0.12	2.22	2.85	0.92	2.02	-63.5
$10_1^+$	1.61	1.60	0.64	0.16	2.22	2.93	0.85	1.99	-69.8
$12_3^+$	1.62	1.66	0.56	0.16	2.22	3.04	0.77	1.97	-60.4
$14_3^+$	1.38	1.47	0.58	0.57	2.47	2.94	1.02	1.57	-77.0
$16_1^+$	1.51	1.85	0.52	0.12	2.26	2.83	0.90	2.02	-62.3
$12_1^+$	1.26	1.22	0.75	0.78	2.57	2.86	1.15	1.42	-87.8
$14_1^+$	1.27	1.17	0.59	0.98	2.75	3.02	1.08	1.16	-88.6
$16_1^+$	1.28	1.19	0.61	0.98	2.82	2.82	1.20	1.17	-91.6
$18_1^+$	1.20	1.17	0.61	1.03	2.89	2.76	1.24	1.11	-94.3
$18_2^+$	0.67	0.73	0.65	1.95	2.19	3.03	0.69	2.10	-83.3
$20_1^+$	0.75	0.84	0.51	1.90	2.20	2.89	0.76	2.15	-86.2
$22_1^+$	0.70	0.90	0.46	1.94	2.34	2.70	0.86	2.11	-88.6
$24_1^+$	0.87	1.12	0.01	2.00	2.41	2.33	1.23	2.03	-93.9
$26_1^+$	0.88	1.12	0.00	2.00	2.09	2.64	1.21	2.06	-89.0
$0_2^+$	1.72	1.68	0.49	0.11	2.52	3.07	1.30	1.12	
$2_2^+$	1.71	1.63	0.57	0.09	2.98	3.57	1.22	0.22	+7.8
$4_3^+$	1.75	1.61	0.54	0.10	3.14	3.71	0.93	0.22	+41.8
$6_2^+$	1.72	1.61	0.56	0.11	3.05	3.59	1.15	0.21	+12.0
$4_2^+$	1.67	1.34	0.90	0.09	3.05	3.55	1.19	0.21	-42.8
$8_3^+$	1.62	1.69	0.49	0.20	2.24	2.80	1.00	1.96	-59.2
$10_2^+$	1.41	1.41	0.65	0.54	2.34	3.02	1.01	1.64	-76.1
$12_2^+$	1.29	1.22	0.69	0.80	2.52	3.10	1.01	1.38	-85.1

state  $12_1^+$ , the  $1p1n$  aligned band appears in the yrast line of  $14_1^+$ ,  $16_1^+$  and  $18_1^+$  like  $^{66}\text{Ge}$ . There seems to be strong coupling between the  $2n$  and  $1p1n$  aligned bands at  $J = 12$ . The third band crossing takes place between  $J = 18$  and  $J = 20$ . The  $2p2n$  aligned band takes the lowest position from  $20_1^+$  to  $26_1^+$ . Figure 8 shows that the aligned nucleons in the  $g_{9/2}$  orbit couple to  $T = 1$ ,  $J = 8$  in the  $2n$  aligned band ( $8_1^+$ ,  $10_1^+$ ),  $T = 0$ ,  $J = 9$  in the  $1p1n$  aligned band ( $14_1^+$ ,  $16_1^+$ ,  $18_1^+$ ) and  $T = 0$ ,  $J = 16$  in the  $2p2n$  aligned band ( $20_1^+$ ,  $22_1^+$ ,  $\dots$ ,  $26_1^+$ ). We show the successive four bands in the  $E_x - J$  graph, in Fig. 9, where corresponding experimental bands are taken from Ref. [11]. The agreement between theory and experiment is satisfactory. It should be noted that the correspondence between theory and experiment is good for the non-yrast states as well as the yrast states.

However, the  $12_1^+$  state is assigned as the  $J = 12$  member of the band on  $8_1^+$  in the experiment [11], while the  $12_1^+$  state resembles the  $1p1n$  aligned state rather than the  $2n$  aligned state in our calculation. The  $J - \omega$  graph for the even- $J$  positive-parity yrast states of  $^{68}\text{Ge}$  (Fig. 5(a)) shows an insufficient description of the energy difference  $E(18_1^+) - E(16_1^+)$ . The calculated  $B(E2)$  values between different bands do not agree with the experi-

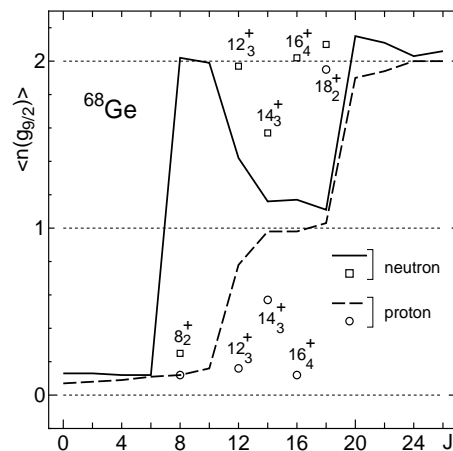


FIG. 7: The expectation values of neutron and proton numbers in the  $g_{9/2}$  orbit ( $\langle n_{g_{9/2}}^\nu \rangle$  and  $\langle n_{g_{9/2}}^\pi \rangle$ ) for the even- $J$  positive-parity yrast states (lines) and some other states (marks) of  $^{68}\text{Ge}$ .

mental  $B(E2)$  values in Table I, either. These discrepancies reveal missing correlations in our model Hamiltonian, and suggest stronger interplays between the different bands near the band crossings. Still, the calculated  $J - \omega$  graph in Fig. 5(a) and the  $E_x - J$  graph in Fig. 9 trace the trends of the experimental graphs. We can attribute the changes in these graphs to the successive band crossings indicated in Figs. 7 and 8.

So far, we have used the word “alignment” for the maximum angular momentum coupling in the  $g_{9/2}$  or-

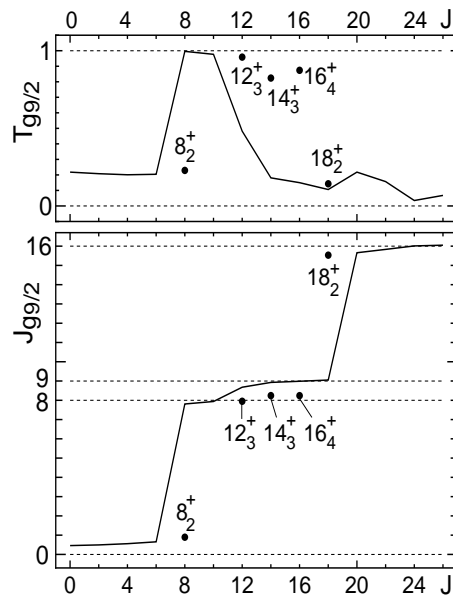


FIG. 8: The expectation values of the spin and isospin of nucleons in the  $g_{9/2}$  orbit ( $J_{g_{9/2}}$  and  $T_{g_{9/2}}$ ) for the even- $J$  positive-parity yrast states (lines) and some other states (marks) of  $^{68}\text{Ge}$ .

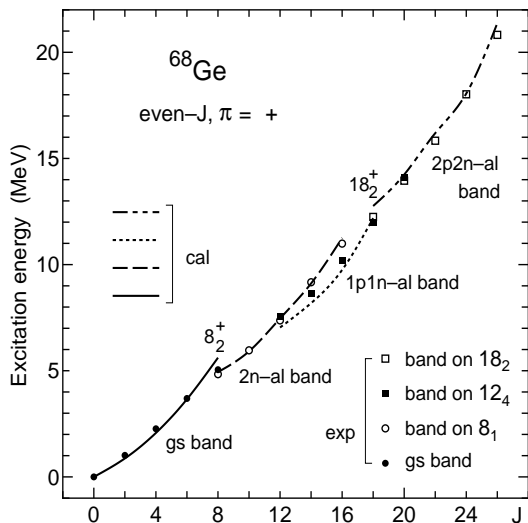


FIG. 9: Comparison of the calculated four bands with the experimentally observed bands for  $^{68}\text{Ge}$ .

bit. How is the angular momentum coupling of the aligned particles in the  $g_{9/2}$  orbit with the central system excluding the  $g_{9/2}$  particles? We calculated expectation values of the spin and isospin of the central system which is represented by nucleons in the  $pf$  shell ( $2p_{3/2}$ ,  $1f_{5/2}$ ,  $2p_{1/2}$ ) in our shell model. We write these expectation values as  $J_{pf}$  and  $T_{pf}$ , and evaluate them using the relations  $J_{pf} = [(\langle \hat{j}_{pf} \rangle^2) + 1/4]^{1/2} - 1/2$  and  $T_{pf} = [(\langle \hat{t}_{pf} \rangle^2) + 1/4]^{1/2} - 1/2$ , where  $\hat{j}_{pf}$  and  $\hat{t}_{pf}$  mean the spin and isospin operators for the subspace ( $2p_{3/2}$ ,  $1f_{5/2}$ ,  $2p_{1/2}$ ). Calculated  $J_{pf}$  and  $T_{pf}$  together with  $J_{g_{9/2}}$  and  $T_{g_{9/2}}$  are illustrated in Fig. 10. Figure 10 indicates that the spin of the aligned particles in the  $g_{9/2}$  orbit actually aligns with the spin of the central system in the  $2n$ ,  $1p1n$  and  $2p2n$  aligned bands. This situation can be called a system composed of a rotor and particles. We can see some deviation from the weak coupling of the rotor and particles near  $J = 8$  in Fig. 10. The upper panel of Fig. 10 indicates vector coupling of the isospins  $T_{pf}$  and  $T_{g_{9/2}}$  for the  $2n$  aligned yrast states with  $T = 1$ ,  $8_1^+$  and  $10_1^+$ . It should be noticed that the residual nucleons in the  $pf$  shell coupled with the aligned  $1p1n$  pair with  $T = 0$ ,  $J = 9$  must have the isospin  $T = 1$  for the nucleus  $^{66}\text{Ge}$ , while the residual nucleons coupled with the aligned  $2n$  pair with  $T = 1$ ,  $J = 8$  can have the isospins  $T = 0$  and  $T = 1$ . This effect is seen in the upper panel of Fig. 10. The different isospin couplings bring about different properties to the  $1p1n$  and  $2n$  aligned bands. The problem is related to the competition between the  $T = 1$  and  $T = 0$  pair correlations in the central system which is represented by the  $pf$ -shell nucleons in our shell model.

The superiority of the  $J = 9$ ,  $T = 0$   $1p1n$  pair in the  $14_1^+$ ,  $16_1^+$  and  $18_1^+$  states can be attributed to the condition that the  $T = 0$ ,  $J = 9$   $pn$  interaction is stronger than the  $T = 1$ ,  $J = 8$  interaction. Note that while the

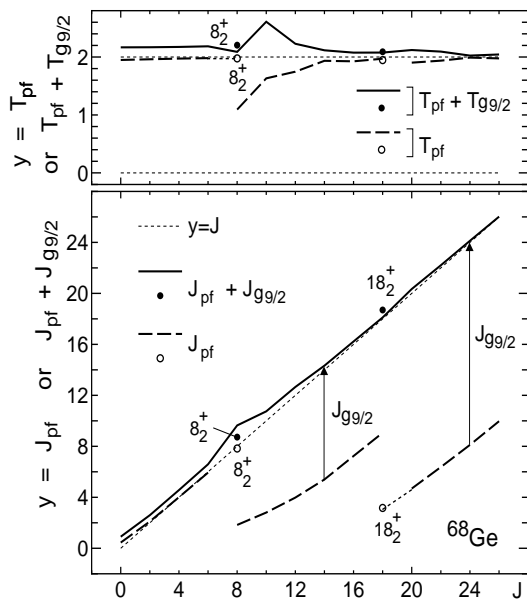


FIG. 10: The expectation values of spins  $J_{pf}$  and  $J_{g_{9/2}}$ , and those of isospins  $T_{pf}$  and  $T_{g_{9/2}}$ , for the even- $J$  positive-parity yrast states (lines) and some other states (marks) of  $^{68}\text{Ge}$ .

$T = 1$ ,  $J = 2j - 1$  interaction is repulsive, the  $T = 0$ ,  $J = 2j$  interaction is very attractive in ordinary effective interactions. If we set  $\langle (g_{9/2})^2 | V | (g_{9/2})^2 : T = 0, J = 9 \rangle$  zero, the  $1p1n$  aligned states do not become the yrast states, while the  $gs$  band is hardly disturbed.

What conditions cause such a nearly pure  $1p1n$  alignment? In Ref. [33], we investigated even-mass Ru isotopes around  $^{90}\text{Ru}$  which is symmetrical to  $^{66}\text{Ge}$  with respect to the particle-hole transformation in the  $(p_{3/2}, f_{5/2}, p_{1/2}, g_{9/2})$  space. We did not find any sign of the  $T = 0$   $1p1n$  alignment there, and could not see a pure  $2n$  alignment at the backbending state  $8_1^+$  in  $^{90}\text{Ru}$ . An important thing is that the Fermi level lies at the  $g_{9/2}$  orbit itself in the Ru isotopes but considerably far from the  $g_{9/2}$  orbit in the Ge isotopes. The appearance of the nearly pure  $2n$  and  $1p1n$  alignments in  $^{66}\text{Ge}$  is based on the condition that the high-spin orbit  $g_{9/2}$  is quite apart from the Fermi level and has the opposite parity to the  $pf$  shell. Only even-number nucleons are allowed to occupy the  $g_{9/2}$  orbit after covering the cost of excitation energy from  $pf$  to  $g_{9/2}$ . We can expect the  $T = 0$   $1p1n$  alignment in  $N \approx Z$  even-even nuclei near the Ge isotopes.

Carrying out the same shell model calculation, we explored other nuclei  $^{64}\text{Ge}$ ,  $^{70}\text{Ge}$ ,  $^{60-68}\text{Zn}$  and  $^{68}\text{Se}$  for the  $T = 0$   $1p1n$  alignment. The calculation for  $^{64}\text{Ge}$  predicts that the  $1p1n$  alignment takes place at  $12_1^+$  just above the  $gs$  band from  $0_1^+$  to  $10_1^+$  and continues till  $18_1^+$ , but there is no  $2n$  aligned state in the even- $J$  positive-parity yrast states. For  $^{70}\text{Ge}$ , on the other hand, the calculation yields only one  $1p1n$  aligned yrast state,  $16_1^+$ . The results suggest that the  $1p1n$  aligned state is favored when the

neutron excess  $N - Z$  is small, especially when  $N = Z$ . This is probably related to the existence of suitable low-energy states in the  $A - 2$  subsystem excluding the  $1p1n$  pair  $(g_{9/2})_{J=9, T=0}^2$ , for instance, such as the  $T = 0$  states of  $^{62}\text{Ga}$  for  $^{64}\text{Ge}$  and the  $T = 1$  states of  $^{64}\text{Ga}$  for  $^{66}\text{Ge}$ . We got the  $T = 0$   $1p1n$  aligned states  $14_1^+$  and  $16_1^+$  above the  $gs$  band ( $0_1^+ - 10_1^+$ ) for  $^{62}\text{Zn}$ , while we have no  $1p1n$  aligned state in the even- $J$  positive-parity yrast states for the Zn isotopes with  $A > 62$ . It is interesting that the states  $10_1^+$  and  $12_1^+$  are the  $T = 1$   $1p1n$  aligned states but the  $14_1^+$  state is the  $T = 0$   $1p1n$  aligned state in our calculation for  $^{60}\text{Zn}$ , although the extended  $P+QQ$  model may not be good enough for the four valence-nucleon system [26]. The  $^{68}\text{Se}$  nucleus has the maximum dimension in the present shell model calculations, i.e., about  $1.6 \times 10^8$  for  $0_1^+$ . The calculation predicts the early  $T = 0$   $1p1n$  alignment at  $10_1^+$ , namely, the  $T = 0$   $1p1n$  aligned states from  $10_1^+$  to  $18_1^+$  above the  $gs$  band ( $0_1^+ - 8_1^+$ ). We can expect the existence of the  $T = 0$   $1p1n$  aligned states in  $^{70}\text{Se}$  and  $^{72}\text{Se}$  similar to  $^{66}\text{Ge}$  and  $^{68}\text{Ge}$ , but we did not make calculations because of large dimensions.

The expectation values of proton and neutron numbers in the four orbits are tabulated also for the second band on  $2_2^+$  observed in  $^{66}\text{Ge}$ , in Table III. Table III shows that the states  $2_2^+$ ,  $4_2^+$  and  $6_2^+$  (see Figs. 1 and 4(a)) have no aligned nucleons in the  $g_{9/2}$  orbit. There is not a notable difference between the low-spin states up to  $J = 6$  of the  $gs$  and second bands with respect to the distribution of nucleons. The  $8_2^+$  state has the aligned  $2n$  pair in the  $g_{9/2}$  orbit as mentioned above. The experiment for  $^{68}\text{Ge}$  [11] found a cascade of decay  $8_2^+ (or\ 8_3^+) \rightarrow 6_2^+ \rightarrow 4_3^+ \rightarrow 2_3^+ \rightarrow 0_2^+$  in addition to the sequence  $6_2^+ \rightarrow 4_2^+ \rightarrow 2_2^+$ . A similar decay scheme could be found for  $^{66}\text{Ge}$ . The low-spin excited band near above the  $gs$  band should be investigated further, but we leave the investigation except for the nuclear shape discussed later.

## B. Particle alignments in other yrast states

Let us get onto the subject of other yrast states with positive and negative parities ( $\pi = \pm$ ) of  $^{66}\text{Ge}$  and  $^{68}\text{Ge}$ .

The odd- $J$  positive-parity yrast states of  $^{66}\text{Ge}$  are interesting because of the cascade  $\Delta J = 1$  transitions on the  $11_1^+$  state [6]. We have discussed it in section III B. For these odd- $J$  states, we show calculated data about their wave-functions in Appendix A: the occupation probabilities and  $Q$  moments in Table V; The expectation values of the spin and isospin of nucleons occupying the  $g_{9/2}$  orbit,  $J_{g_{9/2}}$  and  $T_{g_{9/2}}$ , in Fig. 17. Table V shows that a structural change takes place at  $11_1^+$  and the states  $11_1^+$ ,  $13_1^+$ ,  $15_1^+$ ,  $17_1^+$  and  $19_1^+$  have a common structure. The common structure is created by the  $T = 0$ ,  $J = 9$   $1p1n$  alignment in the  $g_{9/2}$  orbit, as known from Fig. 17. We can now understand the almost equivalent two  $J - \omega$  graphs from  $13_1^+$  to  $19_1^+$  and from  $14_1^+$  to  $18_1^+$  in Fig. 4(a) (see the dotted and solid lines). The odd- $J$  states  $11_1^+$  to  $19_1^+$  have the structure of the

$T = 0$ ,  $J = 9$   $1p1n$  alignment which is the same as that of the even- $J$  states  $14_1^+$  to  $18_1^+$ . It should be remembered that the  $12_1^+$  state resembles the  $1p1n$  aligned state rather than the  $2n$  aligned state. The cascade  $\Delta J = 1$  transitions  $15_1^+ \rightarrow 14_1^+ \rightarrow 13_1^+ \rightarrow 12_1^+ \rightarrow 11_1^+$  can be related to the common structure between the odd- $J$  and even- $J$  states in our model, which is in disagreement with the consideration of possible four-quasiparticle structure in Ref. [6]. The large value of  $B(M1 : 12_1^+ \rightarrow 11_1^+)$  in our calculation seems to be related to the strong mixing of the  $1p1n$  and  $2n$  aligned states at  $12_1^+$ . The mixing of the  $1p1n$  and  $2n$  aligned bands could affect  $B(M1)$  values for other states and hence the cascade  $\Delta J = 1$  transitions.

It is notable that the  $T = 1$ ,  $J = 8$   $2n$  aligned states do not become the yrast states when  $J = \text{odd}$  and  $\pi = +$  in  $^{66}\text{Ge}$ . This may be related to kinematic effects in the spin and isospin couplings. The calculation predicts that the yrast states  $21_1^+$ ,  $23_1^+$  and  $25_1^+$  are the  $2p2n$  aligned states with  $J_{g_{9/2}} \approx 16$  and  $T_{g_{9/2}} \approx 0$ . We have the  $1p1n$  aligned band on  $11_1^+$  and the  $2p2n$  aligned band on  $21_1^+$  in addition to the low-spin band with no alignment, for the odd- $J$  positive-parity yrast states of  $^{66}\text{Ge}$ . Let

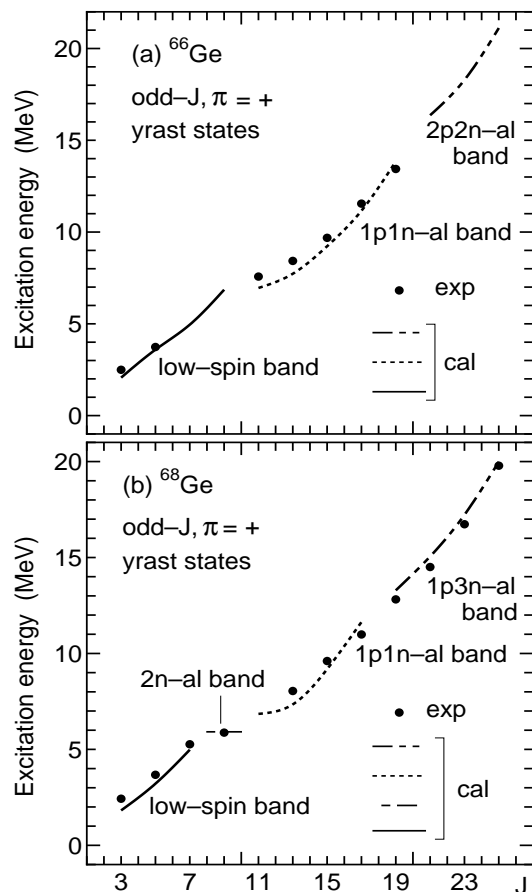


FIG. 11: Comparison of the calculated odd- $J$  positive-parity yrast states (curves) with the experimental ones (solid circles) for (a)  $^{66}\text{Ge}$  and (B)  $^{68}\text{Ge}$ .

us take a glance at the  $E_x - J$  graph in Fig. 11(a) to compare it with a corresponding figure of  $^{68}\text{Ge}$  in the lower panel (b). Although the experimental data are not sufficient for comparison, the good reproduction of the  $J - \omega$  graph from  $13_1^+$  to  $17_1^+$  in Fig. 4(a) supports our classification.

For  $^{68}\text{Ge}$ , odd- $J$  positive-parity yrast states are experimentally observed up to  $25_1^+$ . We show calculated data about their wave-functions in the same manner as that for  $^{66}\text{Ge}$ , in Table VI and Fig. 18 of Appendix A. Table VI indicates successive three types of particle aligned bands above the low-spin band with no alignment. They are the  $T = 1, J = 8$   $2n$  aligned band which has only one yrast state  $9_1^+$ , the  $T = 0, J = 9$   $1p1n$  aligned band from  $11_1^+$  to  $17_1^+$  and the one-proton-three-neutron ( $1p3n$ ) aligned band from  $19_1^+$  to  $25_1^+$ , as known from Fig. 18. Interestingly, the two excess neutrons in  $^{68}\text{Ge}$  as compared with  $^{66}\text{Ge}$  produce another type of particle alignment in the  $g_{9/2}$  orbit for the odd- $J$  positive-parity yrast states with  $J \geq 19$ . The  $1p3n$  aligned states have the combination of  $T = 1$   $2n$  pair and  $T = 0$   $pn$  pair in the  $g_{9/2}$  orbit which produces the spin  $J_{g_{9/2}} = 9/2^\pi + (9/2 + 7/2 + 5/2)^\nu = 15$  and the isospin  $T_{g_{9/2}} = 1$ . The calculation reproduces well the experimental  $J - \omega$  graph for the  $J \geq 15$  states except  $17_1^+$ , as mentioned for Fig. 5(a). Thus, we have the four bands for the odd- $J$  positive-parity yrast states of  $^{68}\text{Ge}$ , as shown in the  $E_x - J$  graph of Fig. 11(b). The calculation traces quite well the experimental footprints in Fig. 11(b).

There are sufficient data on the negative-parity yrast states of  $^{66}\text{Ge}$  and  $^{68}\text{Ge}$  except for  $J = \text{even}$  of  $^{66}\text{Ge}$ . The negative-parity states have odd-number nucleons in the  $pf$  shell with  $\pi = -$  and hence at least one nucleon must occupy the  $g_{9/2}$  orbit in the even-mass Ge isotopes. This condition produces different structures from those of the positive-parity states in  $^{66}\text{Ge}$  and  $^{68}\text{Ge}$ .

First, we consider the odd- $J$  negative-parity yrast states of  $^{66}\text{Ge}$  which are experimentally observed up to tentative  $23_1^-$ . We show calculated data about their wave-functions in Table VII and Fig. 19 of Appendix B. Table VII indicates that the low-spin states up to  $13_1^-$  have approximately one nucleon in the  $g_{9/2}$  orbit, giving the spin  $J_{g_{9/2}} \approx 9/2$  and the isospin  $T_{g_{9/2}} \approx 1/2$ . At  $15_1^-$ , one proton and two neutrons ( $1p2n$ ) align in the  $g_{9/2}$  orbit and produce the spin  $J_{g_{9/2}} = 9/2^\pi + (9/2 + 7/2)^\nu = 25/2$  and the isospin  $T_{g_{9/2}} = 1/2$ . The  $1p2n$  aligned band continues up to  $23_1^-$  where the band terminates. The  $1p2n$  aligned states can be regarded as the  $T = 1$  aligned  $2n$  pair coupled with one proton and also as the  $T = 0$  aligned  $pn$  pair coupled with one neutron. We cannot distinguish the two types of coupling. By the way, the  $2p2n$  aligned states are forbidden by the condition that the nucleon number in the  $g_{9/2}$  orbit must be odd. The next particle-aligned state is the two-proton-three-neutron ( $2p3n$ ) aligned state  $25_1^-$  as predicted in the bottom line of Table VII. The sequence of the odd- $J$  negative-parity yrast states has two bands, the low-spin

band with one neutron in the  $g_{9/2}$  orbit and the  $1p2n$  aligned band on  $15_1^-$ , which is illustrated in Fig. 12(a). The theoretical two bands nicely trace the experimental footprints. We have discussed in section III B that the calculated  $B(E2)$  values recommend us to regard the  $19_2^-$  and  $21_2^-$  states as the members of the band on  $15_1^-$  (see Fig. 1). We plot two curves for the band on  $15_1^-$  in Fig. 12(a). One is the curve connecting the yrast states  $15_1^-$  to  $23_1^-$  and the other is the curve passing the states  $19_2^-$  and  $21_2^-$ .

Secondly, we consider the odd- $J$  negative-parity yrast states of  $^{68}\text{Ge}$ . The calculated data about their wave-functions are given in Table VIII and Fig. 20 of Appendix B. Table VIII and Fig. 20 show that the odd- $J$  negative-parity yrast states of  $^{68}\text{Ge}$  have essentially the same features as those of  $^{66}\text{Ge}$  with respect to the particle alignments in the  $g_{9/2}$  orbit. There are two bands, the low-spin band with one neutron in the  $g_{9/2}$  orbit and the  $1p2n$  aligned band which starts from  $15_1^-$  and terminates at  $23_1^-$ . In the  $1p2n$  aligned band, the three nucleons in the  $g_{9/2}$  orbit have  $J_{g_{9/2}} \approx 25/2$  and  $T_{g_{9/2}} \approx 1/2$ . We show the  $E_x - J$  graph in Fig. 12(b). The agreement

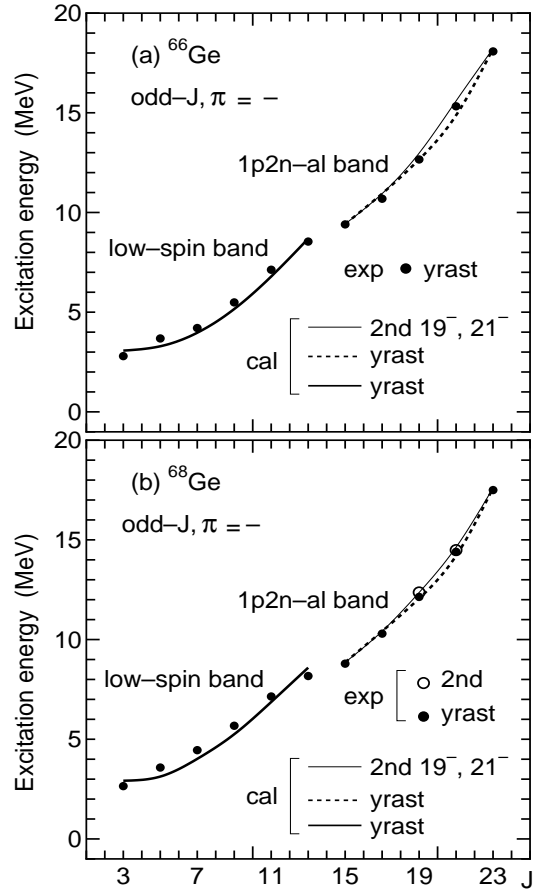


FIG. 12: Comparison of the calculated odd- $J$  negative-parity yrast states (curves) with the experimental ones (circles) for (a)  $^{66}\text{Ge}$  and (b)  $^{68}\text{Ge}$ .

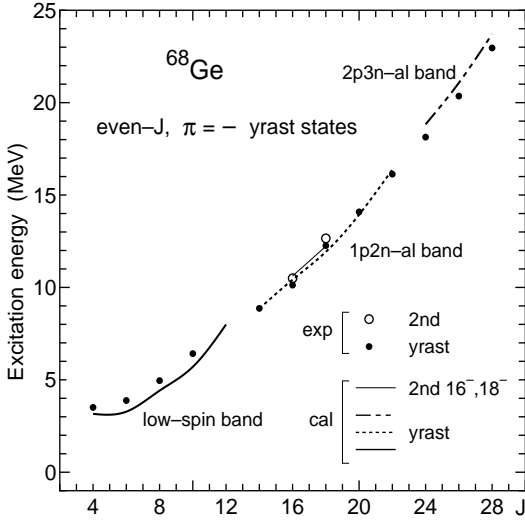


FIG. 13: Comparison of the calculated even- $J$  negative-parity states (curves) with the experimental ones (circles) for  $^{68}\text{Ge}$ .

between theory and experiment is good especially for the  $1p2n$  aligned band on  $15_1^-$ . We have discussed the continuation of bands near  $19_1^-$  and  $21_1^-$  in section III B. The calculated  $B(E2)$  values have recommended us to regard the states  $17_1^-$ ,  $19_2^-$ ,  $21_2^-$  and  $23_1^-$  as members of the band on  $15_1^-$ . The curve connecting these states appears to be smoother in Fig. 12(b), although this assignment is not necessarily consistent with the assignment of bands in the experiment [11]. We note that the  $19_2^-$  and  $21_2^-$  states have the  $1p2n$  alignment in the  $g_{9/2}$  orbit.

Thirdly, let us look at the even- $J$  negative-parity yrast states of  $^{68}\text{Ge}$ . The maximum spin  $J^\pi = 28^-$  is experimentally observed in this sequence. We show calculated data about their wave-functions in Table IX and Fig. 21 of Appendix B. Table IX and Fig. 21 indicate that the even- $J$  negative-parity yrast states up to  $22_1^-$  have a similar nature to the odd- $J$  negative-parity yrast states up to  $23_1^-$  in  $^{68}\text{Ge}$ . The calculated high-spin states from  $14_1^-$  to  $22_1^-$  contain the aligned three nucleons ( $1p2n$ ) with  $J_{g_{9/2}} \approx 25/2$  and  $T_{g_{9/2}} \approx 1/2$  in the  $g_{9/2}$  orbit. This is consistent with the discussion in Ref. [11] that there are very low-lying aligned  $14^-$  and  $16^-$  states with one  $g_{9/2}$  proton and two  $g_{9/2}$  neutrons. The calculated  $B(E2)$  values for the  $18^- \rightarrow 16^-$  transitions are  $0.7 e^2\text{fm}^4$  for  $18_1^- \rightarrow 16_1^-$  and  $209 e^2\text{fm}^4$  for  $18_1^- \rightarrow 16_2^-$ , which suggests discontinuity of the  $1p2n$  aligned states between  $16_1^-$  and  $18_1^-$ . This is also consistent with no detection of the  $18_1^- \rightarrow 16_1^-$  transition in the experiment [11]. For the higher-spin states  $24_1^-$ ,  $26_1^-$  and  $28_1^-$ , Fig. 21 indicates the  $2p3n$  alignment coupled to  $J_{g_{9/2}} = (9/2 + 7/2)^\pi + (9/2 + 7/2 + 5/2)^\nu = 37/2$  and  $T_{g_{9/2}} = 1/2$  in the  $g_{9/2}$  orbit. These states are the members of the  $2p3n$  aligned band. This assignment is supported by the calculated  $B(E2)$  values, a small value for the transition  $24_1^- \rightarrow 22_1^-$  (which shows discontinuity between the states  $22_1^-$  and  $24_1^-$ ) and large values for the

transitions  $28_1^- \rightarrow 26_1^- \rightarrow 24_1^-$ . Tables VII and VIII show that there could be the  $2p3n$  aligned states with  $J = \text{odd}$ ,  $\pi = -$  above  $23_1^-$  both in  $^{66}\text{Ge}$  and  $^{68}\text{Ge}$ . We have three bands in the even- $J$  negative-parity yrast states of  $^{68}\text{Ge}$ , the low-spin band with one neutron in the  $g_{9/2}$  orbit, the  $1p2n$  aligned band on  $14_1^-$  and the  $2p3n$  aligned band on  $24_1^-$ , as shown in the  $E_x - J$  graph of Fig. 13. The agreement between theory and experiment is not good for the low-spin band but is satisfactorily good for the  $1p2n$  and  $2p3n$  aligned bands.

We close this subsection by noting that the structural changes at the band crossings in Figs. 11-13 manifest themselves in the changes of the spectroscopic  $Q$  moment (see Tables V-IX in Appendixes A and B).

## V. DEPENDENCE OF THE FIRST BAND CROSSING ON NEURON NUMBER

We have seen the change of the first band crossing (backbending point) from  $^{66}\text{Ge}$  to  $^{68}\text{Ge}$ . The backbend-

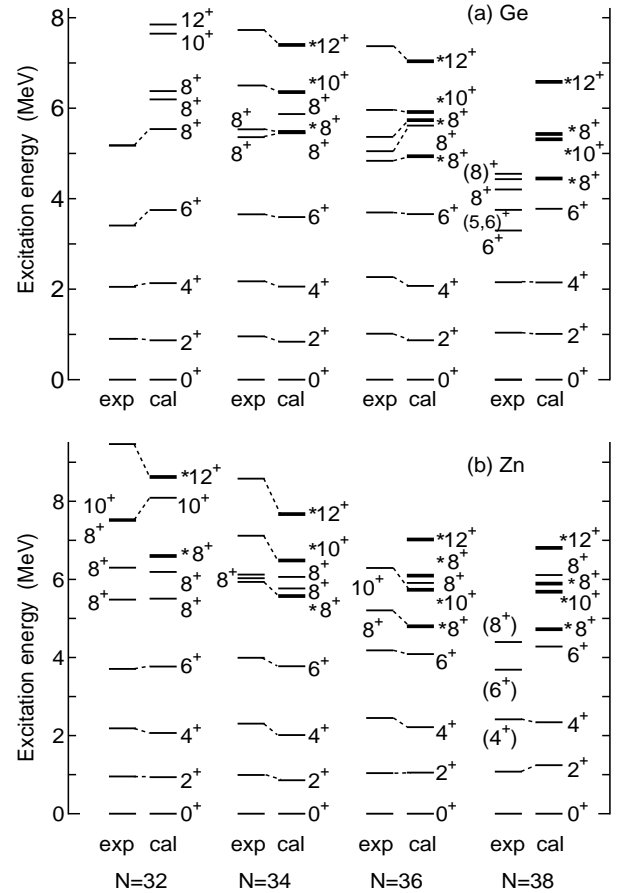


FIG. 14: Changes of the low-energy levels in the (a) Ge and (b) Zn isotopes. The  $2n$  and  $1p1n$  aligned states (thick lines) are distinguished with the asterisks from the members of the  $gs$  band.

ing takes place at  $10_1^+$  in  $^{66}\text{Ge}$  and  $8_1^+$  in  $^{68}\text{Ge}$ . This phenomenon is explained in terms of the  $2n$  alignment in the previous section. Namely, it is caused by the competition between the  $gs$  band and the  $2n$  aligned band for holding the lowest (yrast) position in energy near  $J = 8$ . Let us illustrate the competition in the Ge isotopes including  $^{64}\text{Ge}$  and  $^{70}\text{Ge}$ , in Fig. 14(a). We calculated energy levels of  $^{64}\text{Ge}$  and  $^{70}\text{Ge}$  using the same Hamiltonian as that for  $^{66}\text{Ge}$  and  $^{68}\text{Ge}$ . The force strengths in Eq. (3) are too strong for the  $gs$  band of the  $N = Z$  nucleus  $^{64}\text{Ge}$ , pushing up the energy levels as  $J$  increases. The present model is, however, good enough to discuss the band crossing near  $J = 8$ . The  $2n$  aligned states  $8^+$  and  $10^+$ , and the  $12^+$  state with dominant component of the  $1p1n$  alignment are denoted by the thick lines with the asterisks (as  $*8^+$ ) in Fig. 14(a).

In Fig. 14(a), while the experimental  $6_1^+$  state goes up gradually till  $^{68}\text{Ge}$  with  $N = 36$ , the  $8_1^+$  state reaches the peak at  $^{66}\text{Ge}$  with  $N = 34$  and goes down as  $N$  increases. (The  $6_1^+$  state is not successfully reproduced for  $^{70}\text{Ge}$  with  $N = 38$ .) The calculation indicates that the  $2n$  aligned  $8_1^+$  state does not intrude among the lowest three  $8^+$  states when  $N = 32$ , but competes with the  $8^+$  member of the  $gs$  band when  $N = 34$  and becomes lower in energy than the latter when  $N \geq 36$ . It should be noticed that the  $N$ -dependent behaviors of energy levels of the Ge isotopes are reproduced by the  $N$ -independent parameters of interactions. We can say that the first band crossing depends on the neutron number. This feature can be attributed to the upward movement of the neutron Fermi level with the increase in the neutron number  $N$ . The approach of the Fermi level to the  $g_{9/2}$  orbit makes nucleons be easy to go into the  $g_{9/2}$  orbit and to get high spin by particle alignment.

The same behavior is observed in the Zn isotopes as shown in Fig. 14(b). Here, we strengthened the force strengths for the Zn isotopes by setting  $A = 62$  in Eq. (3). We use the same ( $N$ -independent) force strengths for the Zn isotopes with  $A = 62 - 68$ . The experimental  $6_1^+$  state goes up gradually till  $N = 36$ . The  $8_1^+$  state reaches the peak at  $N = 34$  and goes down as  $N$  increases. The change in the Zn isotopes shows a slight difference from that in the Ge isotopes. In  $^{64}\text{Zn}$  with  $N = 34$ , the  $2n$  aligned  $8^+$  state is lower than the  $8^+$  member of the  $gs$  band, but the backbending takes place at  $10_1^+$  like  $^{66}\text{Ge}$  with  $N = 34$ . The backbending at  $8_1^+$  is observed at  $N = 36$  also in the Zn isotopes. We can see the same behavior of the  $8_1^+$  state in the Se isotopes as those in the Zn and Ge isotopes. The explanation for the backbending at  $8_1^+$  when  $N = 36$  mentioned for the Ge isotopes, that the position of the neutron Fermi level affects whether the  $2n$  alignment in the  $g_{9/2}$  orbit is easy or not, is therefore reasonable. The common behavior depending on the neutron number supports our conclusion that the first band crossing (backbending) at  $8_1^+$  is caused by the  $2n$  alignment in the  $g_{9/2}$  orbit.

## VI. NUCLEAR SHAPES OF GE ISOTOPES

The nuclear shape or the coexistence of oblate and prolate shapes has been a hot topic in nuclei around Ge isotopes [6, 19, 20, 21, 22, 23]. The VAMPIR calculations gave positive (oblate)  $Q$  moments to the  $gs$  band and negative (prolate)  $Q$  moments to the second low-spin band in  $^{68}\text{Ge}$  [13, 14, 15]. The recent calculations [6, 21] also yielded the deepest minimum for an oblate shape and the next minima for prolate shapes in  $^{68}\text{Ge}$  and  $^{66}\text{Ge}$ , and predicted shape coexistence and  $\gamma$  softness.

In order to investigate this problem, we calculated spectroscopic  $Q$  moments of all the states of  $^{66}\text{Ge}$  and  $^{68}\text{Ge}$ , which are listed in Tables III-IX. Our model yields negative  $Q$  moments for the  $gs$  band and other states, except for the  $2_2^+$  and  $4_3^+$  states of  $^{66}\text{Ge}$  and the  $2_2^+$ ,  $4_3^+$  and  $6_2^+$  states of  $^{68}\text{Ge}$ . Certainly we obtain the coexistence of the prolate and oblate shapes in the Ge isotopes, but the oblate shape narrowly appears in the second or third excited state ( $2^+$ ,  $4^+$  or  $6^+$ ) of  $^{66}\text{Ge}$  and  $^{68}\text{Ge}$  in our calculations. This suggests that the oblate minimum is shallower than the prolate minimum in the potential energy surface. Our result disagrees with the VAMPIR result [13, 14, 15]. A notable difference between our model and the VAMPIR model is in the single-particle energies. The  $g_{9/2}$  level lies below the  $p_{1/2}$  level in the VAMPIR model. We calculated the spectroscopic  $Q$  moment by setting  $\varepsilon_{g_{9/2}} = \varepsilon_{p_{1/2}}$ , but could not get positive  $Q$  moments for the  $gs$  band. We also examined the  $Q$  moment by changing the force parameters  $g_0$ ,  $\chi_2$  and  $\chi_3$ . However, changing the parameters does not affect the signs of the  $Q$  moments within the limit that the energy levels are not seriously damaged. The present model therefore predicts the prolate shape for the  $gs$  band and other states except for the narrow appearance of the oblate shape in a few low-spin excited states in  $^{66}\text{Ge}$  and  $^{68}\text{Ge}$ .

The  $Q$  moment of the  $2_1^+$  state ( $Q(2_1^+)$ ) has not experimentally been observed for  $^{66}\text{Ge}$  and  $^{68}\text{Ge}$  yet, but was measured for  $^{70}\text{Ge}$ . To examine our model and to see the variation of  $Q(2_1^+)$  and  $Q(2_2^+)$  depending on the neutron number, we calculated  $Q$  moments for  $^{70}\text{Ge}$  and  $^{64}\text{Ge}$ . The calculation for  $^{64}\text{Ge}$  yields negative  $Q$  moments for the  $gs$  band and exceptionally yields a positive  $Q$  moment for the  $2_2^+$  state, which is similar to the results for  $^{66}\text{Ge}$  and  $^{68}\text{Ge}$ . In  $^{70}\text{Ge}$ , on the contrary, the  $2_1^+$  and  $4_1^+$  states have positive  $Q$  moments, while the  $2_2^+$  state has a negative  $Q$  moment. Let us illustrate the variations of  $Q(2_1^+)$  and  $Q(2_2^+)$  in the Ge isotopes from  $^{64}\text{Ge}$  ( $N = 32$ ) to  $^{70}\text{Ge}$  ( $N = 38$ ), in Fig. 15(a). The  $Q(2_1^+)$  value calculated for  $^{70}\text{Ge}$  is in good agreement with the experimental value, in Fig. 15(a). This agreement suggests that the present predictions for  $Q(2_1^+)$  and  $Q(2_2^+)$  are better than those of Refs. [13, 14, 15]. There are two data on  $Q(2_1^+)$  for Zn isotopes, *i.e.*, for  $^{64}\text{Zn}$  and  $^{68}\text{Zn}$ . We calculated  $Q$  moments for the Zn isotopes from  $^{62}\text{Zn}$  ( $N = 32$ ) to  $^{68}\text{Zn}$  ( $N = 38$ ). Calculated results are shown in Fig. 15(b). This figure also indicates the success of our model in reproducing the experimental  $Q(2_1^+)$  values

of  $^{64}\text{Zn}$  and  $^{68}\text{Zn}$ , which supports our prediction for the  $Q$  moments of the Ge isotopes. It is probable that in contrast to the suggestions of Refs. [6, 13, 14, 15] the  $2_1^+$  state of the  $gs$  band is prolate in  $^{66}\text{Ge}$  and  $^{68}\text{Ge}$  and oblate in  $^{70}\text{Ge}$ , while the  $2_2^+$  state has an opposite shape against the  $2_1^+$  state in these nuclei.

Figure 15(a) shows a gradual decrease of the prolate (oblate) deformation of the  $2_1^+$  ( $2_2^+$ ) state from  $^{66}\text{Ge}$  to  $^{68}\text{Ge}$  and shape inversions of the  $2_1^+$  and  $2_2^+$  states in  $^{70}\text{Ge}$ . Similar decreases of the prolate and oblate deformations of the  $2_1^+$  and  $2_2^+$  states from  $^{64}\text{Zn}$  to  $^{68}\text{Zn}$  are seen in Fig. 15(b). There seems to be a trend that the prolate (oblate) shape of the  $2_1^+$  ( $2_2^+$ ) state tends toward the oblate (prolate) shape when the neutron number goes over  $N = 34$ . This trend is clearer in the Ge isotopes with two more protons than in the Zn isotopes. It, therefore, must be related also to the proton number. In Ref. [34], we investigated the shape transition from the prolate shape of  $^{64}\text{Ge}$  to the oblate shape of  $^{68}\text{Se}$ , and showed that the increase of the nucleon number in the  $2p_{1/2}$  orbit ( $\langle n_{p_{1/2}} \rangle$ ) contributes to the oblate deformation. The acceleration of the shape variation from the Zn isotopes to the Ge isotopes can be attributed to the occupation of the  $2p_{1/2}$  orbit by protons as well as neutrons. The shape variation seen in Fig. 15(a) (Fig. 15(b)) corresponds to the increase of the neutron number in the  $2p_{1/2}$  orbit, as shown in Tables III and IV (incidentally,  $\langle n_{p_{1/2}}^v \rangle$  is 1.48 for the  $2_1^+$  state of  $^{70}\text{Ge}$ ). This must be related to the upward movement of the neutron Fermi level from  $N = 34$  to  $N = 38$ , which causes the

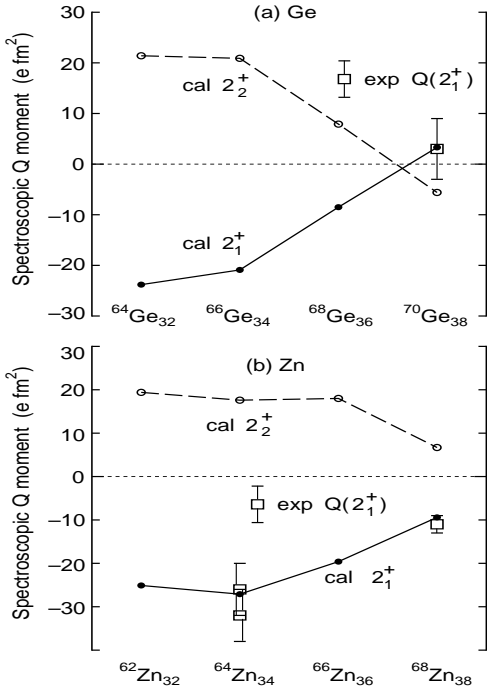


FIG. 15: Comparison between calculated and experimental  $Q$  moments in the (a) Ge and (b) Zn isotopes.

lowering of the  $2n$  aligned  $8_1^+$  state from  $^{66}\text{Ge}$  to  $^{70}\text{Ge}$  as discussed in the last section.

Let us investigate further the nuclear shapes of the Ge isotopes and the shape variation by using an alternative method, the CHF method [35, 36]. We consider the constrained Hamiltonian with the following quadratic terms of quadrupole moment  $q_M$  and spin  $J$ :

$$H' = H + c_1 \sum_{M=0,\pm 2} (\langle Q_{2M} \rangle - q_M)^2 + c_2 [\langle J_x \rangle - \sqrt{J(J+1)}]^2, \quad (5)$$

$$q_0 = \sqrt{\frac{5}{4\pi}} q \cos \gamma, \quad q_{\pm 2} = \sqrt{\frac{5}{8\pi}} q \sin \gamma, \quad (6)$$

where  $c_1$  and  $c_2$  are predefined positive constants, and  $J_x$  denotes the  $x$ -component of the angular momentum operator. We plot the energy surface  $\langle q, \gamma | H | q, \gamma \rangle_{J=0}$  in the  $q - \gamma$  plane for  $^{66}\text{Ge}$ ,  $^{68}\text{Ge}$  and  $^{70}\text{Ge}$ , in Fig. 16. In Fig. 16(a) for  $^{66}\text{Ge}$ , the energy surface has a minimum near  $q \approx 56 \text{ fm}^2$  and  $\gamma \approx 0^\circ$ , suggesting an axially symmetric prolate deformation with  $\beta \approx 0.2$ . This value  $\beta \approx 0.2$ , which is consistent with the calculated  $B(E2)$  value  $B(E2: 2_1^+ \rightarrow 0_1^+) \approx 281 e^2 \text{ fm}^4$  on the assumption of the axial symmetry, corresponds with previous predictions  $\beta \approx 0.2 - 0.22$  [6, 22]. The energy surface in Fig. 16(a), however, displays a valley along the  $\gamma$  direction, which means  $\gamma$  softness of  $^{66}\text{Ge}$  like  $^{64}\text{Ge}$  (see Ref. [34]).

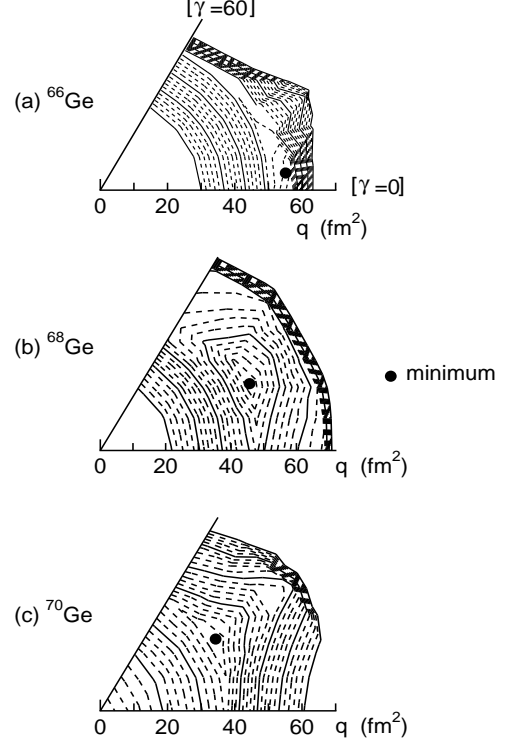


FIG. 16: The energy surface  $\langle q, \gamma | H | q, \gamma \rangle_{J=0}$  in the  $q - \gamma$  plane ( $0^\circ \leq \gamma \leq 60^\circ$ ) plotted with contours, for (a)  $^{66}\text{Ge}$ , (b)  $^{68}\text{Ge}$  and (c)  $^{70}\text{Ge}$ .

The energy surface for  $^{68}\text{Ge}$  indicates a triaxial deformation in Fig. 16(b). The minimum is near  $q \approx 50 \text{ fm}^2$  and  $\gamma \lesssim 30^\circ$  in the  $q - \gamma$  plane. This seems to be consistent with the small prolate deformation obtained by the shell model calculation, from the relation  $Q \propto -q \cos(3\gamma)$  in the Davydov model. The energy surface for  $^{70}\text{Ge}$  also shows a triaxial deformation in Fig. 16(c). The minimum near  $q \approx 45 \text{ fm}^2$  and  $\gamma \gtrsim 30^\circ$  in the  $q - \gamma$  plane corresponds to the small oblate deformation known from the experimental  $Q$  moment  $Q(2_1^+)$ .

The CHF calculations thus support the above discussions which are based on the shell model calculations of  $Q(2_1^+)$ . The energy surface calculations interpret the shape variation depending on the neutron number from  $^{66}\text{Ge}$  to  $^{70}\text{Ge}$  as the movement along the  $\gamma$  direction (crossing the  $\gamma = 30^\circ$  border) with a gradual decrease of quadrupole deformation in the  $q - \gamma$  plane. A similar trend is seen in the CHF results for the Zn isotopes from  $^{64}\text{Zn}$  to  $^{68}\text{Zn}$ , although the minimum point for  $^{68}\text{Zn}$  does not cross the  $\gamma = 30^\circ$  border. Our figures of the energy surfaces for  $^{66}\text{Ge}$  and  $^{68}\text{Ge}$  do not correspond with those of the TRS calculations [6]. The discrepancy is probably due to the difference between the two Hamiltonians used in our calculations and the TRS ones. Our Hamiltonian describes well the energy levels and other properties of  $^{66}\text{Ge}$  and  $^{68}\text{Ge}$ , and also the  $Q$  moments observed in  $^{70}\text{Ge}$ ,  $^{64}\text{Zn}$  and  $^{68}\text{Zn}$ , as we have seen.

## VII. SUMMARY

We have investigated the structure of  $^{66}\text{Ge}$  and  $^{68}\text{Ge}$ , by carrying out large scale shell model calculations with the extended  $P + QQ$  Hamiltonian in the configuration space  $(2p_{3/2}, 1f_{5/2}, 2p_{1/2}, 1g_{9/2})$ . The shell model reproduces excellently the energy levels of  $^{66}\text{Ge}$  and  $^{68}\text{Ge}$ , and also satisfactorily those of  $^{64}\text{Ge}$ ,  $^{65}\text{Ge}$ ,  $^{67}\text{Ge}$  and  $^{70}\text{Ge}$  ( $^{62}\text{Zn}$ ,  $^{64}\text{Zn}$ ,  $^{66}\text{Zn}$  and  $^{68}\text{Zn}$ ). The model explains well the graphs of spin versus angular frequency for the positive- and negative-parity yrast states with even  $J$  and odd  $J$ , and quite well the experimental  $B(E2)$  values, in  $^{66}\text{Ge}$  and  $^{68}\text{Ge}$ . The calculated  $B(E2)$  values are basically consistent with the band schemes assigned by  $\gamma$  transitions in the experiments [6, 11].

To analyze the structure, we calculated the expectation values of proton and neutron numbers in the four orbits, the expectation values of the spin and isospin of nucleons in the  $pf$  shell  $(2p_{3/2}, 1f_{5/2}, 2p_{1/2})$  and in the  $g_{9/2}$  orbit, and the spectroscopic  $Q$  moment. The analysis has clarified that the structural changes in the four sequences of the positive- and negative-parity yrast states with even  $J$  and odd  $J$  are caused by various types of particle alignments in the  $g_{9/2}$  orbit. Although not all the predicted aligned states have been found, the calculations explain the experimental graphs of the excitation energy versus spin as shown in Figs. 6, 9, 11-13. The results are summarized as follows.

(A)  $^{66}\text{Ge}$ :

(1) The even- $J$ ,  $\pi = +$  sequence has the four bands up to  $26_1^+$ : the  $gs$  band,  $2n$  aligned band,  $1p1n$  aligned band and  $2p2n$  aligned band. (2) The odd- $J$ ,  $\pi = +$  sequence has the three bands up to  $25_1^+$ : the low-spin band,  $1p1n$  aligned band and  $2p2n$  aligned band. (3) The odd- $J$ ,  $\pi = -$  sequence has the two bands up to  $23_1^-$ : the low-spin band and  $1p2n$  aligned band.

(B)  $^{68}\text{Ge}$ :

(1) The even- $J$ ,  $\pi = +$  sequence has the four bands up to  $26_1^+$ : the  $gs$  band,  $2n$  aligned band,  $1p1n$  aligned band and  $2p2n$  aligned band. (2) The odd- $J$ ,  $\pi = +$  sequence has the four bands up to  $25_1^+$ : the low-spin band,  $2n$  aligned state,  $1p1n$  aligned band and  $1p3n$  aligned band. (3) The odd- $J$ ,  $\pi = -$  sequence has the two bands up to  $23_1^-$ : the low-spin band and  $1p2n$  aligned band. (4) The even- $J$ ,  $\pi = -$  sequence has the three bands up to  $28_1^-$ : the low-spin band,  $1p2n$  aligned band and  $2p3n$  aligned band.

The backbending takes place at  $10_1^+$  in  $^{66}\text{Ge}$  and at  $8_1^+$  in  $^{68}\text{Ge}$ , which is explained by crossing of the  $2n$  aligned band and the  $gs$  band in our calculations. We have discussed that the change of the first band crossing depending on the neutron number, which is observed in the Ge, Zn and Se isotopes, can be attributed to the movement of the neutron Fermi level toward the  $g_{9/2}$  orbit.

We have looked into the nuclear shapes of the Ge isotopes at low energy where no particle alignment takes place. The calculations predict the coexistence of prolate and oblate shapes in the Ge isotopes as follows. The  $2_1^+$  state is prolate in  $^{66}\text{Ge}$  and  $^{68}\text{Ge}$  and oblate in  $^{70}\text{Ge}$ , while the  $2_2^+$  state has an opposite shape against the  $2_1^+$  state in these nuclei. The prolate (oblate) deformation of the  $2_1^+$  ( $2_2^+$ ) state decreases from  $^{66}\text{Ge}$  to  $^{68}\text{Ge}$  and the shape inversions of the  $2_1^+$  and  $2_2^+$  states happen in  $^{70}\text{Ge}$ . The CHF calculations interpret the shape variation depending on the neutron number as the movement along the  $\gamma$  direction (crossing the  $\gamma = 30^\circ$  border) with a gradual decrease of quadrupole deformation in the  $q - \gamma$  plane. The prediction is supported by the agreement between the calculated and experimental  $Q$  moments ( $Q(2_1^+)$ ) in  $^{70}\text{Ge}$ ,  $^{64}\text{Zn}$  and  $^{68}\text{Zn}$ .

The  $1f_{7/2}$  orbit is not included in our calculations because the extension of configuration space makes the shell model calculations impossible. This truncation ought to have effects on the results obtained. The  $2d_{5/2}$  orbit possibly affects the results at high energy. Better interaction parameters would be necessary for describing nuclei in a wider region.

**APPENDIX A: STRUCTURE OF THE ODD- $J$  POSITIVE-PARITY YRAST STATES**

TABLE V: The proton and neutron numbers  $\langle n_a^\pi \rangle$  and  $\langle n_a^\nu \rangle$ , and calculated  $Q$  moments (in  $e \text{ fm}^2$ ), for the odd- $J$  positive-parity yrast states of  $^{66}\text{Ge}$ .

$^{66}\text{Ge}$	proton				neutron				$Q$
	$p_{3/2}$	$f_{5/2}$	$p_{1/2}$	$g_{9/2}$	$p_{3/2}$	$f_{5/2}$	$p_{1/2}$	$g_{9/2}$	
$3_1^+$	1.79	1.56	0.56	0.10	2.44	2.72	0.70	0.14	-0.9
$5_1^+$	1.71	1.79	0.43	0.07	2.35	2.83	0.69	0.12	-17.9
$7_1^+$	1.75	1.76	0.41	0.09	2.21	2.87	0.78	0.13	-7.3
$9_1^+$	1.76	1.80	0.35	0.09	2.21	2.87	0.78	0.14	-14.8
$11_1^+$	1.24	1.14	0.61	1.02	1.90	2.49	0.56	1.06	-77.9
$13_1^+$	1.30	1.12	0.57	1.01	1.79	2.58	0.59	1.04	-82.6
$15_1^+$	1.30	1.14	0.55	1.01	1.79	2.45	0.72	1.04	-86.4
$17_1^+$	1.24	1.17	0.58	1.01	1.77	2.22	0.97	1.03	-89.0
$19_1^+$	1.23	1.16	0.59	1.02	1.67	2.17	1.13	1.04	-91.2
$21_1^+$	0.67	0.93	0.49	1.92	1.53	1.71	0.65	2.11	-81.4
$23_1^+$	0.60	1.06	0.39	1.96	1.36	1.94	0.65	2.05	-83.4
$25_1^+$	0.46	1.07	0.51	1.96	1.37	2.06	0.50	2.07	-84.3

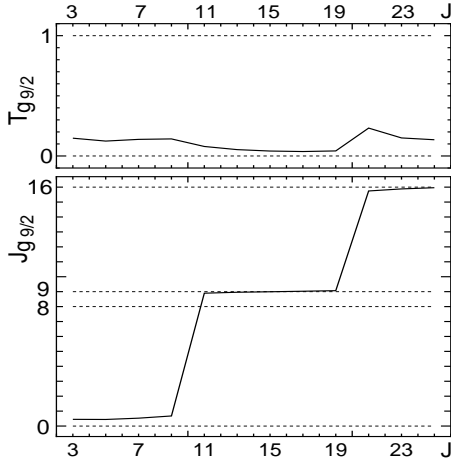


FIG. 17: The expectation values of spin and isospin,  $J_{g9/2}$  and  $T_{g9/2}$ , for the odd- $J$  positive-parity yrast states of  $^{66}\text{Ge}$ .

TABLE VI: The proton and neutron numbers  $\langle n_a^\pi \rangle$  and  $\langle n_a^\nu \rangle$ , and calculated  $Q$  moments (in  $e \text{ fm}^2$ ), for the odd- $J$  positive-parity yrast states of  $^{68}\text{Ge}$ .

$^{68}\text{Ge}$	proton				neutron				$Q$
	$p_{3/2}$	$f_{5/2}$	$p_{1/2}$	$g_{9/2}$	$p_{3/2}$	$f_{5/2}$	$p_{1/2}$	$g_{9/2}$	
$3_1^+$	1.76	1.58	0.57	0.10	3.00	3.54	1.25	0.21	+0.05
$5_1^+$	1.71	1.51	0.68	0.10	3.03	3.49	1.27	0.21	-15.7
$7_1^+$	1.75	1.61	0.53	0.12	3.05	3.39	1.33	0.23	-8.3
$9_1^+$	1.61	1.60	0.64	0.16	2.22	2.93	0.85	1.99	-48.9
$11_1^+$	1.23	1.20	0.61	0.96	2.70	3.00	1.13	1.16	-84.4
$13_1^+$	1.23	1.18	0.54	1.01	2.58	3.17	1.17	1.08	-90.5
$15_1^+$	1.19	1.17	0.63	1.02	2.58	3.20	1.16	1.07	-94.6
$17_1^+$	1.19	1.27	0.55	1.00	2.70	3.05	1.12	1.13	-79.3
$19_1^+$	1.28	1.11	0.55	1.07	1.71	2.64	0.68	2.97	-86.6
$21_1^+$	1.27	1.13	0.53	1.07	1.75	2.51	0.79	2.96	-89.8
$23_1^+$	1.18	1.15	0.55	1.12	1.79	2.30	1.01	2.91	-92.4
$25_1^+$	1.06	1.13	0.56	1.26	1.69	2.32	1.21	2.78	-93.1

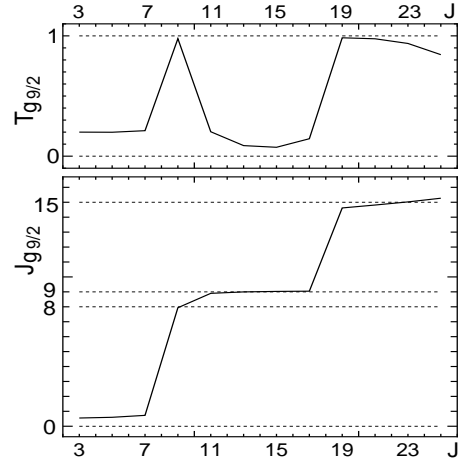


FIG. 18: The expectation values of spin and isospin,  $J_{g9/2}$  and  $T_{g9/2}$ , for the odd- $J$  positive-parity yrast states of  $^{68}\text{Ge}$ .

**APPENDIX B: STRUCTURE OF THE  
NEGATIVE-PARITY YRAST STATES**

TABLE VII: The proton and neutron numbers  $\langle n_a^\pi \rangle$  and  $\langle n_a^\nu \rangle$ , and calculated  $Q$  moments (in  $e \text{ fm}^2$ ), for the odd- $J$  negative-parity yrast states and some other states of  $^{66}\text{Ge}$ .

$^{66}\text{Ge}$	proton				neutron				$Q$
	$p_{3/2}$	$f_{5/2}$	$p_{1/2}$	$g_{9/2}$	$p_{3/2}$	$f_{5/2}$	$p_{1/2}$	$g_{9/2}$	
$3_1^-$	1.58	1.67	0.48	0.27	2.16	2.22	0.72	0.91	-37.8
$5_1^-$	1.60	1.69	0.54	0.18	2.21	2.22	0.59	0.98	-48.0
$7_1^-$	1.64	1.64	0.55	0.17	1.94	2.43	0.67	0.96	-47.9
$9_1^-$	1.64	1.64	0.58	0.14	1.90	2.46	0.65	0.98	-51.0
$11_1^-$	1.66	1.79	0.46	0.09	1.87	2.46	0.65	1.03	-46.4
$13_1^-$	1.60	1.91	0.41	0.08	1.86	2.46	0.64	1.04	-49.2
$15_1^-$	1.29	1.14	0.55	1.02	1.50	1.89	0.60	2.01	-87.7
$17_1^-$	1.29	1.15	0.55	1.02	1.55	1.75	0.69	2.01	-91.1
$19_1^-$	1.29	1.15	0.53	1.03	1.36	2.04	0.61	2.00	-86.7
$19_2^-$	1.22	1.19	0.58	1.01	1.56	1.45	0.98	2.01	-94.6
$21_1^-$	1.28	1.14	0.55	1.03	1.32	2.08	0.61	1.99	-89.0
$21_2^-$	1.20	1.18	0.59	1.03	1.44	1.39	1.17	2.00	-96.5
$23_1^-$	1.26	1.14	0.58	1.03	1.31	2.09	0.58	2.01	-91.1
$25_1^-$	0.78	1.03	0.17	2.02	1.15	1.28	0.59	2.99	-84.9

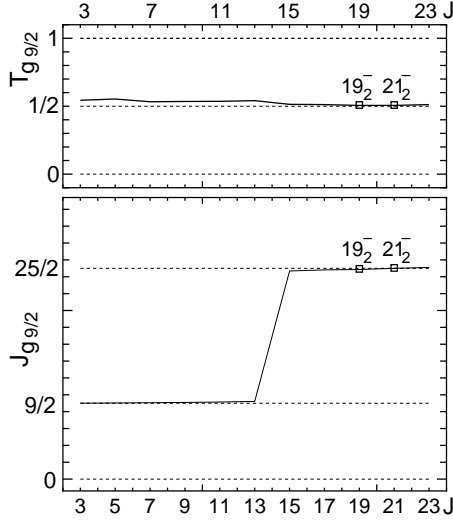


FIG. 19: The expectation values of spin and isospin,  $J_{g9/2}$  and  $T_{g9/2}$ , for the odd- $J$  negative-parity yrast states (lines) and some other states (marks) of  $^{66}\text{Ge}$ .

TABLE VIII: The proton and neutron numbers  $\langle n_a^\pi \rangle$  and  $\langle n_a^\nu \rangle$ , and calculated  $Q$  moments (in  $e \text{ fm}^2$ ), for the odd- $J$  negative-parity yrast states and some other states of  $^{68}\text{Ge}$ .

$^{68}\text{Ge}$	proton				neutron				$Q$
	$p_{3/2}$	$f_{5/2}$	$p_{1/2}$	$g_{9/2}$	$p_{3/2}$	$f_{5/2}$	$p_{1/2}$	$g_{9/2}$	
$3_1^-$	1.61	1.61	0.51	0.28	2.57	3.35	1.12	0.96	-40.5
$5_1^-$	1.60	1.65	0.55	0.20	2.57	3.37	1.04	1.03	-54.8
$7_1^-$	1.67	1.60	0.61	0.13	2.69	3.20	1.04	1.06	-57.7
$9_1^-$	1.67	1.55	0.68	0.10	2.76	3.04	1.10	1.11	-67.5
$11_1^-$	1.57	1.39	0.94	0.10	2.78	2.94	1.18	1.12	-70.9
$13_1^-$	1.45	1.60	0.87	0.08	2.91	2.78	1.18	1.13	-70.2
$15_1^-$	1.26	1.17	0.55	1.02	2.22	2.78	0.97	2.03	-92.6
$17_1^-$	1.25	1.14	0.59	1.02	2.20	2.97	0.79	2.04	-91.8
$19_1^-$	1.26	1.19	0.53	1.02	2.38	2.41	1.17	2.03	-96.2
$19_2^-$	1.26	1.15	0.58	1.02	2.15	2.95	0.86	2.04	-91.1
$21_1^-$	1.18	1.18	0.62	1.02	2.39	2.34	1.24	2.03	-99.2
$21_2^-$	1.22	1.16	0.59	1.02	2.15	2.76	1.05	2.04	-92.8
$23_1^-$	1.24	1.15	0.59	1.02	2.09	2.67	1.20	2.05	-94.3
$25_1^-$	0.78	0.99	0.22	2.01	1.85	2.29	0.86	3.00	-85.1

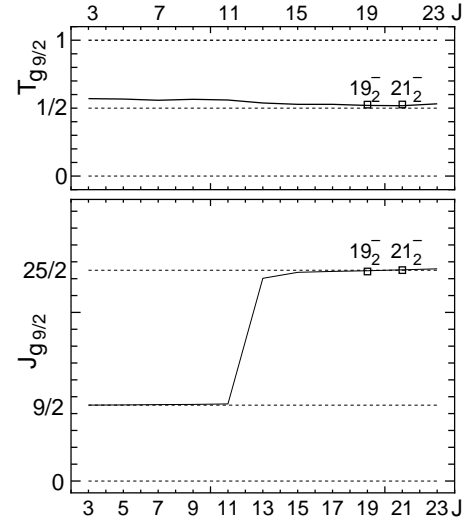


FIG. 20: The expectation values of spin and isospin,  $J_{g9/2}$  and  $T_{g9/2}$ , for the odd- $J$  negative-parity yrast states (lines) and some other states (marks) of  $^{68}\text{Ge}$ .

TABLE IX: The proton and neutron numbers  $\langle n_p^\pi \rangle$  and  $\langle n_n^\nu \rangle$ , and calculated  $Q$  moments (in  $e \text{ fm}^2$ ), for the even- $J$  negative-parity yrast states and some other states of  $^{68}\text{Ge}$ .

$^{68}\text{Ge}$	proton				neutron				$Q$
	$p_{3/2}$	$f_{5/2}$	$p_{1/2}$	$g_{9/2}$	$p_{3/2}$	$f_{5/2}$	$p_{1/2}$	$g_{9/2}$	
$4_1^-$	1.70	1.75	0.47	0.08	2.79	2.87	1.24	1.11	-44.0
$6_1^-$	1.70	1.73	0.49	0.08	2.65	3.12	1.15	1.09	-56.7
$8_1^-$	1.69	1.52	0.69	0.10	2.65	3.15	1.10	1.09	-66.0
$10_1^-$	1.51	1.27	1.13	0.09	2.54	3.20	1.18	1.08	-74.5
$12_1^-$	1.63	1.61	0.67	0.09	2.76	2.97	1.14	1.13	-52.7
$14_1^-$	1.26	1.17	0.55	1.02	2.22	2.78	0.97	2.04	-74.1
$16_1^-$	1.25	1.14	0.59	1.02	2.20	2.97	0.79	2.04	-75.6
$16_2^-$	1.17	1.23	0.58	1.02	2.24	2.93	0.79	2.04	-81.7
$18_1^-$	1.21	1.16	0.60	1.02	2.13	2.92	0.92	2.03	-89.2
$18_2^-$	1.21	1.18	0.54	1.08	2.23	2.71	1.06	2.00	-88.7
$20_1^-$	1.22	1.22	0.51	1.05	2.37	2.61	1.00	2.01	-85.9
$22_1^-$	1.03	1.72	0.24	1.02	2.41	2.38	1.18	2.04	-81.0
$24_1^-$	0.70	0.86	0.44	2.01	1.73	2.46	0.80	3.01	-86.6
$26_1^-$	0.74	1.00	0.26	2.00	1.71	2.31	0.97	3.01	-88.7
$28_1^-$	0.89	1.10	0.00	2.01	1.56	2.21	1.23	3.01	-90.2
$30_1^-$	0.03	1.00	0.00	2.97	1.42	1.99	0.55	4.03	-61.8

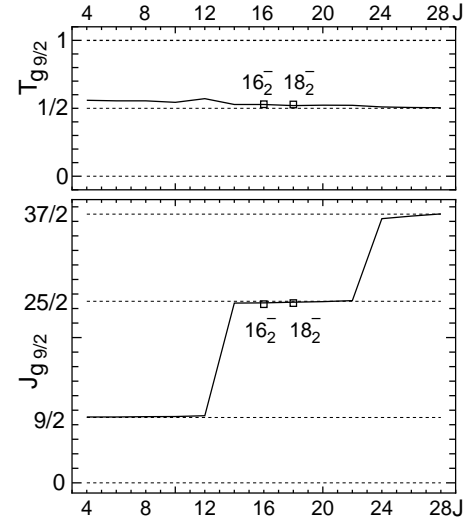


FIG. 21: The expectation values of spin and isospin,  $J_{g_{9/2}}$  and  $T_{g_{9/2}}$ , for the even- $J$  negative-parity yrast states (lines) and some other states (marks) of  $^{68}\text{Ge}$ .

- [1] E. Nolte, Y. Shida, W. Kutschera, R. Prestele, and H. Morinaga, *Z. Phys.* **268**, 267 (19742).
- [2] L. Cleenmann, J. Eberth, W. Neumann, W. Wiehl, and V. Zobel, *Nucl. Phys.* **A334**, 157 (1980).
- [3] R. Soundranayagam, R.B. Piercey, A.V. Ramayya, J.H. Hamilton, A.Y. Ahmed, H. Yamada, C.F. Maguire, G.L. Bomar, R.L. Robinson, and H.J.Kim, *Phys. Rev. C* **25**, 1575 (1982).
- [4] A. Boucenna, L. Kraus, I. Linck, and Tsan Ung Chan, *Phys. Rev C* **42**, 1297 (1990).
- [5] U. Hermkens, F. Becker, J. Eberth, S. Freund, Mylaeus, S. Skoda, W. Teichert, and A.v.d. Werth, *Z. Phys. A* **343**, 371 (1992).
- [6] E.A. Stefanova *et al.*, *Phys. Rev. C* **67**, 054319 (2003).
- [7] R.C. Pardo, C.N. Davids, M.J. Murphy, E.B. Norman, and L.A. Parks, *Phys. Rev. C* **15**, 1811 (1977).
- [8] A.P. de Lima *et al.*, *Phys. Rev. C* **23**, 213 (1981).
- [9] L. Chaturvedi *et al.*, *Phys. Rev. C* **43**, 2541 (1991).
- [10] L. Chaturvedi *et al.*, *Int. J. Mod. Phys. E* **5**, 1565 (1996).
- [11] D. Ward *et al.*, *Phys. Rev. C* **63**, 014301 (2001).
- [12] M.E. Barclay, *J. Phys. G* **12**, L295 (1986).
- [13] A. Petrovici, K.W. Schmid, F. Gümer, and A. Faessler, *Nucl. Phys.* **A483**, 317 (1988).
- [14] A. Petrovici, K.W. Schmid, F. Gümer, and A. Faessler, *Nucl. Phys.* **A504**, 277 (1989).
- [15] A. Petrovici, K.W. Schmid, F. Gümer, and A. Faessler, *Nucl. Phys.* **A517**, 108 (1990).
- [16] S.T. Hsieh, H.C. Chiang, and Der-San Chuu, *Phys. Rev. C* **46**, 195 (1992).
- [17] Der-San Chuu, S.T. Hsieh, and H.C. Chiang, *Phys. Rev. C* **47**, 183 (1993).
- [18] J.P. Elliott, J.A. Evans, V.S. Lac, and G.L. Long, *Nucl. Phys.* **A609**, 1 (1996).
- [19] R. Bengtsson, P. Möller, J.R. Nix, and J. Zhang, *Phys. Scr.* **29**, 402 (1984).
- [20] W. Nazarewicz, J. Dudek, R. Bengtsson, T. Bengtsson, and I. Ragnarsson, *Nucl. Phys.* **A435**, 397 (1985).
- [21] P. Sarriguren, E. Moya de Guerra, and A. Escuderos, *Nucl. Phys.* **A658**, 13 (1999).
- [22] P.J. Ennis, C.J. Lister, W. Gelletly, H.G. Price, B.J. Varley, P.A. Butler, T. Hoare, S. Cwiok, and W. Nazarewicz, *Nucl. Phys.* **A535**, 392 (1991).
- [23] M. Yamagami, K. Matsuyanagi, and M. Matsuo, *Nucl. Phys.* **A693**, 579 (2001).
- [24] K. Kaneko, M. Hasegawa and T. Mizusaki, *Phys. Rev. C* **66**, 51306(R) (2002).
- [25] M. Hasegawa and K. Kaneko, *Phys. Rev. C* **59**, 1449 (1999).
- [26] M. Hasegawa, K. Kaneko and S. Tazaki, *Nucl. Phys. A* **674**, 411 (2000); **688**, 765 (2001).
- [27] T. Mizusaki, *RIKEN Accel. Prog. Rep.* **33**, 14 (2000).
- [28] M. Hasegawa, K. Kaneko and T. Mizusaki, to be published in *Phys. Rev. C*.
- [29] D. Rudolph *et al.*, *Eur. Phys. J. A* **6**, 377 (1999).
- [30] A. Juodagalvis and S. Åberg, *Nucl. Phys.* **A683**, 206(2001).
- [31] Yang Sun, Jing-ye Zhang, M. Guidry, Jie Meng SoojaeIm, *Phys. Rev. C* **62**, 021601(R) (2000).
- [32] <http://www.nndc.bnl.gov/nndc/ensdf>
- [33] M. Hasegawa, K. Kaneko, T. Mizusaki, and S. Tazaki, *Phys. Rev. C* **69**, 56401 (2004).
- [34] K. Kaneko, M. Hasegawa and T. Mizusaki, submitted to *Phys. Rev. C*.
- [35] T. Mizusaki, T. Otsuka, Y. Utsuno, M. Honma and T. Sebe, *Phys. Rev. C* **59**, R1846 (1999).
- [36] K. Hara, Yang Sun and T. Mizusaki, *Phys. Rev. Lett.* **83**, 1922 (1999).